April 15, 2015

Masashi Niwano
Meteorological Research Institute
Tsukuba 305-0052, Japan
Phone: +81-29-853-8714
FAX: +81-29-855-6936
e-mail: mniwano@mri-jma.go.jp

Prof. van den Broeke
Editor, The Cryosphere

Dear Prof. van den Broeke:

Please find enclosed authors' responses and the revised manuscript entitled "Numerical simulation of extreme snow melt observed at the SIGMA-A site, northwest Greenland, during summer 2012" by M. Niwano et al. [Paper #tc-2014-184] to The Cryosphere. We have revised the manuscript according to the all Reviewer comments. Please note that the revised manuscript attached below is not as same as what I have uploaded into the Interactive Discussion Board (http://www.the-cryosphere-discuss.net/9/495/2015/tcd-9-495-2015-discussion.html). The former is created using latexdiff, whereas the latter file was made without latexdiff. Therefore, line numbers are different from each other, and all line numbers indicated in the authors' responses originally uploaded into the Interactive Discussion Board have been modified here.

We hope that the revised manuscript is suitable for publication. We look forward to hearing from you.

Yours sincerely,

M. Niwano, T. Aoki, S. Matoba, S. Yamaguchi,
T. Tanikawa, K. Kuchiki, and H. Motoyama

Reply to J. King (Reviewer#1)

We sincerely appreciate the reviewer for taking the time to provide quite valuable comments. Below we describe our responses (in black text) point-by-point to each comment (in blue text). In addition we indicate revisions in the updated manuscript by a yellow highlighter together with line numbers. Please also refer to the revised marked-up manuscript uploaded as a supplementary file. In the manuscript, change logs can be tracked.

General Comments

This paper studies surface energy balance and melt at a site in northwest Greenland at a time (July 2012) when record levels of surface melt were occurring across the Greenland Ice Sheet. The surface energy balance (SEB) at the site is characterized using measurements from an automatic weather station (AWS) and corresponding surface melt rates are then calculated. SEB and melt rates are contrasted between the early part of the study period and the latter part, when higher temperatures and enhanced melt were observed. Analysis of the SEB component by component shows that the enhanced melt was associated with increased downwelling longwave radiation (associated with warm, cloudy conditions) together with enhanced downward turbulent fluxes of sensible and latent heat. The measurements made are clearly of good quality and they have been analysed in an appropriate manner, providing significant insight into the drivers of enhanced surface melt at this site. I believe that the paper is suitable for publication in The Cryosphere once the authors have attended to the general comments given below and the specific comments that I have made on an annotated copy of the manuscript.

We appreciate for this positive evaluation. First, we summarize important revisions, which were conducted considering valuable comments from both reviewers, in the updated manuscript.

Major revisions:

First we have modified the input data for the SMAP model in terms of relative humidity. The reviewer argued the necessity to indicate the exact definition of relative humidity. Related with this, Reviewers#2 also suggested that observed relative humidity with respect to water should be corrected after it is converted to relative humidity with respect to ice. We agree with this point, and performed the correction that Reviewer#2 suggested. Accordingly, input data for the SMAP model was modified and recalculations were performed. However, the results of this paper did not change significantly, because the values of relative humidity with respect to water and ice are almost the same under the condition that air temperature is around 0 °C. In reference to this, scores indicating model performance, values of SEB fluxes, and some figures are changed slightly:

(**P17, L20**) 0.53 °C → 0.58 °C

(**P17, L23**) RMSE = 0.85 °C → RMSE = 0.94 °C

(**P17, L23**) ME = 0.55 °C → ME = 0.68 °C

(**P18, L15**) 0.16 → 0.17

(**P24, L25**) 15.2 → 15.3

(**P24, L25**) -13.2 → -18.0

(**P24, L25**) 17.8 → 7.2

(**P24, L26**) +31.0 → +25.2

(**P24, L27**) 102.5 → 96.7

(**P24, L28**) 55.0 → 49.1

(**P24, L28**) 24.9 to 79.9 → 20.1 to 69.2

(**P32, L28**) +31.0 → +25.2

Table1

Figures 6, 7, 8, 9, 10, 11, and 12

Both reviewers pointed out that error analysis investigating the significance of latent heat flux calculated from the 2LM method (air temperature, relative humidity, and wind speed at two profiles are employed to calculate turbulent heat flux at the surface) is necessary. It is because accuracy of air temperature, relative humidity, and wind speed sensors affect calculated latent heat flux with the 2LM method. In the original

manuscript, we only investigated uncertainties induced by the snow surface roughness length for momentum. Now, we have completely understood and agreed with that it is insufficient, because it does not change the sign of latent heat flux but only modified its order, which both reviewers pointed out. In addition, both reviewers commented that the turbulent heat fluxes in the presentation of SEB should be calculated in a consistent manner (only 1LM or 2LM). Based on this consideration, we have reconstructed the paper especially after model evaluation section. Until Sect. 4, basic construction is as same as the original manuscript. After Sect. 5, we first present calculated SEB characteristics, where the turbulent heat fluxes are calculated employing only the 1LM method. Next, we discuss validity of the obtained SEB from various aspects in Sect. 6 "Discussion". In Sect. 6, we begin with investigating the effects of model setting on the SEB calculation (Sect. 6.1). In this subsection, we discussed impacts of the choices of snow surface roughness length and emissivity on the calculated SEB characteristics. The original discussion on the effects of snow surface roughness length has been reconstructed there (basic flow of discussion is as same as the original manuscript, but several corrections of sentences are performed). The motivation of investigating effects of emissivity on the SEB calculation was the comment by Reviewer#2 regarding the validity of the choice of this value. Finally, in Sect. 6.2 (reconstructed from the original Sect. 5 with some minor corrections of sentences), we discussed uncertainties in the 2LM method referring to valuable comments by both reviewers. In conclusion, we could only say that the 1LM method calculated latent heat flux could be underestimated and the 2LM method calculated latent heat flux seemed to be plausible; however, uncertainty involved in the 2LM method was so large that we could not confirm its significance, because gradients of air temperature, vapor pressure, and wind speed between two measurement heights (they were used for the 2LM calculation) were very small. Details of each relevant correction are explained in our responses to all related comments below. Technical corrections related to the reconstruction are as follows:

(**P18, L25**) Sect. 5 → Sect. 6.2

(**P19, L4**) Sect. 5 → Sect. 6.2

(**P24, L6**) Figure 11 → Figure 10

(**P24, L21**) Fig. 12 → Fig. 11

(**P24, L23**) Figure 12 → Figure 11

Figure 10a (**P21, L15**) → Figure 12a (**P28, L12**)

Figure 10c (**P22, L22**) → Figure 12b (**P29, L6**)

Fig. 10c (**P22, L25**) → Fig. 12b (**P29, L9**)

Fig. 10a (**P22, L28**) → Fig. 12a (**P29, L12**)

Fig. 10c (**P23, L10**) → Fig. 12b (**P29, L18**)

Minor revisions:

During revision process, we found a typo at the beginning of Sect. 2 in the original manuscript: "An automated weather station (AWS) was newly installed at site SIGMA-A on 29 ~~July~~ June 2012 (Aoki et al., 2014a)." It is corrected in the updated manuscript. (**P6, L14**)

1.) Manuscript p.8. There is a large discrepancy (nearly a factor of 5) between the precipitation recorded at the site by bucket measurement and the precipitation diagnosed from the reanalysis. In the paper this is simply accounted for by applying a scale factor to the reanalysis precipitation. While one could argue that going further than this is outside the scope of the paper, I think that the authors should discuss possible reasons for the discrepancy. Is this a very local effect (in space and/or time)? I suspect that it may be, because reanalyses appear to reproduce observations of surface mass balance across the Greenland Ice Sheet quite well on longer timescales (e.g. Chen et al., Adv. Atmos. Sci., 2011).

Answer: Thank you very much for the very constructive comment. First of all, we think that the short-time rainfall event reported in this study is caused by a mesoscale convective system, and this kind of system is generally very difficult for hydrostatic global atmospheric models including ERA-Interim, which can calculate climatic accumulation reasonably even over the Greenland ice sheet. In order to reproduce realistic rainfall amount of this event, we think a high-resolution (in time and space) non-hydrostatic atmospheric model is necessary.

In addition, we found that ERA-Interim originally tends to underestimate annual accumulation in the area north of 68°N (Chen et al., 2011), even though ERA-Interim shows close spatial pattern of accumulation to the observations.

Based on the consideration above, we have added following discussion here: "As demonstrated by Chen et al. (2011), ERA-Interim data originally tends to underestimate annual accumulation in the area north of 68°N, even though it shows close spatial pattern of accumulation to the observations over the whole area of GrIS. In addition, it is possible that insufficient horizontal resolution (0.75°) and a hydrostatic atmospheric model, which cannot reproduce a short-time mesoscale convective system realistically in general, might have caused the large discrepancy." (**P9, L26**).

We have added the following reference related with this revision:

Chen, L., Johannessen, O. M., Huijum, W., and Ohmura, A.: Accumulation over the Greenland Ice Sheet as represented in reanalysis data, Adv. Atmos. Sci., 28, 1-9, doi:10.1007/s00376-010-0150-9, 2011.

2.) The authors argue strongly in favour of using 2-level measurements instead of single-level (plus surface) measurements for calculating latent heat flux. The basis of their argument seems to be that single-level measurements fail to generate the large, downward latent heat fluxes that would be associated with surface hoar deposition. This leads them to claim (MS. p. 25) that "...the 2LM method was an effective way to obtain an accurate HL.". Without an independent (eddy covariance) measurement of HL, it is not possible to substantiate this statement. Furthermore, the single-level method was used for sensible heat flux so the values for the two fluxes will be inconsistent. The advantage of the single-level method is that it uses a minimal set of measurements and produces a consistent set of calculated turbulent fluxes and surface temperature. The 2-level method involves measuring the (often small) differences in temperature and mixing ratio between two measurement levels. There will be measurement uncertainties in both temperature (at least 0.1K, probably greater) and relative humidity (at least

5%) at both levels, leading to a large relative uncertainty in the differences and hence the calculated fluxes. The authors should carry out an error analysis to determine the impact of realistic measurement uncertainties on their calculated fluxes. They could then formally determine whether the results of the 2-level calculation differed significantly from those of the single-level calculation. Some discussion of why the two methods produce HL values of opposite signs would also be useful.

Answer: We would like to thank the reviewer's quite insightful suggestions. Especially, the comment that "The 2-level method involves measuring the (often small) differences in temperature and mixing ratio between two measurement levels. " touches the core of the subject. In this comment, the reviewer argued the necessity of error analysis considering the accuracy of each sensor, which the Reviewer#2 also did. Now, we completely agree with their point of view. In the reconstructed manuscript, discussion on disparities between the 1LM and 2LM methods as well as uncertainties involved in the 2LM method are placed in Sect. 6.2. Below we explain how we corresponded against the reviewer's concerns in Sect. 6.2 (originally Sect. 5).

Until the fourth paragraph, a basic flow of discussion is almost the same as the original manuscript, however, several revisions were performed in order to maintain consistency in the manuscript. Then, in the last paragraph of Sect. 6.2, we calculated wind speed, temperature, and moisture gradients (surface and two levels in the atmosphere) as suggested. Obtained gradients for wind speed, air temperature, and vapor pressure between the surface and the lower measurement height (positive downward) were 1.6 s^{-1}, 0.3 °C m^{-1}, and -0.15 hPa m^{-1}, respectively during the IOP. However, those values between the lower and upper measurement heights were nearly 0, except for the case of wind speed: 0.2 s^{-1}. If we focused on the period from 00:10 to 00:20 UTC on 4 July when SMAP_2LM detected the surface hoar, we found that vapor pressure gradients showed opposite signs: -0.13 hPa m^{-1} for the 1LM method and 0.01 hPa m^{-1} for the 2LM method, respectively. This result explains why the 1LM method failed to detect the surface hoar, whereas the 2LM method succeeded in that. However, those gradients between the lower and upper sensors are too low to grasp uncertainties caused by the

sensor accuracy. The accuracy of each sensor and results from relative calibration between the lower and upper sensors are presented here. As a result, our discussion regarding the uncertainties of the 2LM method is now as follows:

"According to Box and Steffen (2001), the uncertainty of the 2LM method increases as the temperature, humidity, and wind speed differences between two measurement heights decrease. These motivated us to investigate the significance of the 2LM method calculated latent heat flux during IOP. In this inquiry, gradients (positive downward) of wind speed, temperature, and vapor pressure between the surface and the lower measurement height, as well as those between the lower and upper measurement heights were investigated at first. Averaged gradients between the surface and the lower measurement height during the IOP were 1.6 s^{-1}, 0.3 °C m^{-1}, and -0.15 hPa m^{-1}, respectively. The value for vapor pressure is very close to that obtained at Summit during 2000–2002 reported by Cullen et al. (2014). On the other hand, averaged gradients between the lower and upper measurement heights were nearly 0, except for the case of wind speed: 0.2 s^{-1}. Focusing on the period from 00:10 to 00:20 UTC on 4 July when SMAP_2LM detected the surface hoar, vapor pressure gradients showed opposite signs: -0.13 hPa m^{-1} for the 1LM method and 0.01 hPa m^{-1} for the 2LM method, respectively. Although this result explains the reason why only the 2LM method succeeded in the surface hoar detection, the latter value is still very small. These make it difficult to assess uncertainties of the 2LM method caused by each sensor as expected. In fact, numerical sensitivity studies with perturbed input parameters considering absolute accuracy of temperature, relative humidity, and wind speed sensors (±0.2 °C, ±2 %, and ±0.3 m s^{-1}, respectively) in the 2LM calculation modified the picture of calculated turbulent heat fluxes drastically in any calculations. Even when relative differences in the accuracy of two sensors at the lower and upper measurement heights were considered (according to our relative calibration of the instruments performed in advance, air temperature and wind speed sensors at two levels showed no significant difference; however, as for relative humidity, the upper sensor tended to be lower by 1.2 % compared to the lower sensor), differences in calculated latent heat flux with perturbed input parameters were quite large. Therefore, we should conclude that underestimation of the latent heat flux calculated with the 1LM method could be

plausible, although the exact order of underestimation was quite hard to detect during this study period." (**P29, L21**)

As for the presentation of SEB in Sect. 5, we have unified the calculation method of turbulent heat fluxes into the 1LM method as mentioned above.

3.) It would be useful to put the observations into the context of the prevailing synoptic meteorology during the observing period. What were the meteorological conditions that led to the higher temperatures and enhanced cloud cover during the latter part of the IOP? Were these conditions exceptional in the context of the long-term climatology?

Answer: This is a good suggestion. After we submitted the original manuscript, several papers presenting the synoptic weather pattern during July 2012 have been published. In the updated manuscript, we explained the large-scale meteorological condition during IOP referring these papers as follows: "Neff et al. (2014) examined synoptic-scale atmospheric conditions over the GrIS during July 2012 from various aspects and summarized notable features as follows: (1) warm air originating from a record North American heat wave (the North American drought of 2012 was the worst since 1895), (2) transitions in the Arctic Oscillation, (3) transport of water vapor via an Atmospheric River over the Atlantic to Greenland, and (4) the presence of warm ocean waters south of Greenland. Bonne et al. (2015) clearly showed that moist air mass was advected northward following a narrow band reaching southern Greenland and then it moved northward along the western Greenland coast around 9 July. Observed features of above mentioned meteorological properties during the IOP at the SIGMA-A site are consistent with these large-scale atmospheric conditions." (**P9, L1**). We intend to refer to "exceptional state" in the context of the long-term climatology by the following part of the revision above: "(1) warm air originating from a record North American heat wave (the North American drought of 2012 was the worst since 1895)".

Added references are:

Neff, W., Compo, G. P., Ralph, F. M., and Shupe, M. D.: Continental heat anomalies and the extreme melting of the Greenland ice surface in 2012 and 1889, J. Geophys. Res. Atmos., 119, 6520-6536, 10.1002/2014JD021470, 2014.

Bonne, J.-L., Steen-Larsen, H. C., Risi, C., Werner, M., Sodemann, H., Lacour, J.-L., Fettweis, X., Cesana, G., Delmotte, M., Cattani, O., Vallelonga, P., Kjær, H. A., Clerbaux, C., Sveinbjörnsdóttir, Á., E., and Masson-Delmotte, V.: The summer 2012 Greenland heat wave: In situ and remote sensing observations of water vapor isotopic composition during an atmospheric river event, J. Geophys. Res. Atmos., 120, 10.1002/2014JD022602, 2015.

Specific comments and technical corrections

P498, L1: "However, a temperature increase is unlikely to be the only cause of surface melt, because surface melt is physically controlled by the surface energy balance (SEB)." →The occurrence of melt is controlled by temperature, its intensity is controlled by SEB

Answer: We intended that a temperature increase cannot always induce surface melt if increased air temperature is still negative. Here we have corrected as follows: "However, a temperature increase cannot induce surface melt if the surface temperature, which is physically controlled by the surface energy balance (SEB), is below 0 °C." **(P4, L3)**

P498, L7: "induces surface melt." → Only if surface temperature = 0degC

Answer: We agree with this point. We have modified the latter half of this sentence as follows ", and a positive sum of these fluxes (net energy flux) induces surface melt only if the surface temperature equals 0 °C" **(P4, L9)**

P501, L9: "The relative humidity" → Clarify whether relative humidities are reported

with respect to water or ice

Answer: The values presented in Fig. 2 are relative humidity with respect to "water". Here we have indicated it is "The relative humidity with respect to water" (**P8, L16**). Also, we indicated that the AWS measured relative humidity with respect to water in beginning of the same section (**P7, L2**). In addition, we have also mentioned that the values in Fig. 2 are relative humidity with respect to water in the caption of Fig. 2 (**Fig. 2**).

Related to this point, as mentioned in the beginning of this response, we realized that our treatment of relative humidity under the condition that air temperature is negative was not sufficient at the initial manuscript, because we had not performed the general (and sometimes quite necessary) correction of relative humidity with respect to ice presented by Anderson (1994) (Comments by Referee#2 also affected this consideration). In the revised manuscript, we have performed the correction against relative humidity with respect to ice converted from observed relative humidity with respect to water. It is now stated in the revised version as follows: "As for relative humidity with respect to water, we converted it into relative humidity with respect ice when air temperature was below 0 °C, and performed the correction presented by Anderson (1994)." (**P7, L9**). It means that the input data for the SMAP model were modified, and we performed recalculation accordingly.

We have added the following reference related with this revision:

Anderson, P. S.: A method for rescaling humidity sensors at temperatures well below freezing, J. Atmos. Oceanic Technol., 11, 1388-1391, doi:10.1175/1520-0426(1994)011<1388:AMFRHS>2.0.CO;2, 1994.

P502, L6: "The comparison indicated that the accumulated precipitation obtained from the ERA-Interim reanalysis data was lower by a factor of 1/4.9. The most prevailing reason for this discrepancy was not a misrepresentation of the true area of rainfall, but just underestimation by the ERA-Interim reanalysis (Fig. 3)." → Why does ERA-Int

underestimate the intensity of the precipitation so badly? Chen et al (Adv. Atmos. Sci., 2011) find that reanalyses provide a good representation of climatological accumulation across the Greenland Ice Sheet.

Answer: Please consider our answer to General comment (1) above.

P502, L22: "depth" → "thickness"

Answer: Corrected as suggested (**P10, L17**).

P504, L10: "precipitation" → Presumably the model requires the phase of the precipitation (rain or snow) as well as the amount? Does SMAP account for the heat flux associated with rain?

Answer: The phase of the precipitation is internally calculated as a function of wet bulb temperature. In the revised manuscript, we have indicated it as follows: "In default configuration, the SMAP model requires precipitation (partitioned in the model into snow and rain by using the algorithm to calculate snow:rain ratios as a function of wet bulb temperature (Yamazaki, 2001)), air pressure, wind speed, air temperature, relative humidity, downward ultraviolet (UV)-visible and near-infrared radiant fluxes, the diffuse components of UV-visible and near-infrared radiant fluxes, downward longwave radiant flux, subsurface heat flux, and the mass concentrations of snow impurities (BC and dust) (Niwano et al., 2012)." (**P12, L9**).

We have added the following reference related with this revision:

Yamazaki, T.: A one-dimensional land surface model adaptable to intensely cold regions and its applications in eastern Siberia, J. Meteorol. Soc. Jpn., 79(6), 1107–1118, doi:10.2151/jmsj.79.1107, 2001.

As for the second question, please consider our answer to the comment for (P516, L2) below.

P506, L1: “minimum” → "small but non-zero" might be clearer than "minimum"

Answer: We have rewritten as suggested (**P13, L28**).

P506, L13: “of” → “for”

Answer: Corrected as suggested (**P14, L14**).

P509, L9: “indicated that the model tended to underestimate the snow temperature profile. However, the SMAP model satisfactorily simulated the temperatures.” → Sounds a bit inconsistent. Can you clarify?

Answer: We agree with the referee’s point of view. The statement is ambiguous. Here we revised simply as follows: “indicated that the model simulated the temperatures reasonably” (**P17, L10**).

P512, L16: “the assumption of the SMAP model that the snow surface is saturated” → It would be better to say "...on the assumption that air at the surface is saturated with respect to ice at the snow surface temperature"

Answer: This is a nice suggestion. We have rewritten as suggested. Please note that the section has been moved to Sect. 6.2 (**P27, L7**) as mentioned at the beginning of our response.

P513, L14: “ΨM, and ΨH” → Ψ-M, H are not "unknown parameters" but are (specified) functions of the (unknown) stability parameter, z/L, which has to be calculated iteratively. You should give a reference for your choice of psi-functions.

Answer: We agree with this point. We have revised the original explanation as follows: “Other parameters are calculated by the same method used by Niwano et al. (2012). The choice of Ψ_M and Ψ_H depends on stability conditions in the atmospheric boundary layer. When the atmosphere is stable, the SMAP model assumes that $\Psi_M = \Psi_H$ and calculates the profile functions according to Holtslag and De Bruin (1988), whereas the SMAP model carries out the calculations with functions determined by Paulson (1970) under unstable conditions.” (**P28, L6**).

Related to this, the following references are now added:

Holtslag, A. A. M., and De Bruin, H. A. R.: Applied modeling of the nighttime surface energy balance over land, J. Appl. Meteorol., 27, 689-704, doi:10.1175/1520-0450(1988)027<0689:AMOTNS>2.0.CO;2, 1988.

Paulson, C. A.: The mathematical representation of wind speed and temperature profiles in the unstable atomospheric surface layer, J. Appl. Meteorol., 9, 857-861, doi: 10.1175/10.1175/1520-0450(1970)009<0857:TMROWS>2.0.CO;2, 1970.

P514, L21: “However, it is still obvious that characteristics of latent heat fluxes with perturbed *z*0 are significantly different from the results from OBS_2LM.” → The most significant difference between 1LM and 2LM is the difference in the sign of HL and no amount of variation of Z0 is going to change this.

Answer: We agree with this point. As explained in the beginning of this response and our answer to the general comment 2), we have investigated difference between the 1LM and 2LM methods in Sect. 6.2 of the updated manuscript, although we could not

determine significant difference between both methods as mentioned in our answer to the general comment 2). The discussion regarding the uncertainties in SEB caused by the choice of snow surface roughness length is now placed in Sect. 6.1 as mentioned in the beginning of this response.

P516, L2: "*H*R is the heat flux associated with rainfall," → You should state how you calculate this

Answer: We have added following description: "H_R is the heat flux associated with rainfall calculated as a function of rainfall rate and a difference in rain temperature (wet bulb temperature is assumed) and surface temperature (Niwano et al., 2012)," (**P23, L21**)

P516, L15: "it increased" → "became generally positive"

Answer: We have rewritten as suggested (**P24, L11**).

P516, L19: "while it was almost 0 Wm^{-2} in the daytime." → Presumably this indicates a near-isothermal snowpack as a result of meltwater percolation?

Answer: Yes, exactly. Additional explanation is given in the updated manuscript: "Finally, H_G showed clear diurnal variation: it heated the surface especially during the night time, while it was almost 0 Wm^{-2} in the daytime as a result of isothermal profile in the near-surface snowpack caused by meltwater percolation." (**P24, L13**).

P516, L21: "it remained positive" → "it remained positive at all times"

Answer: We have added "at all times" as suggested (**P24, L18**).

P518, L24: “comparable and reasonable.” → Not clear what you mean. "Validation results that the model was able to produce a good simulation of the evolution of snow surface temperatures and snow temperature profiles"?

Answer: We agree with point. It can cause misunderstandings. Now, we have revised simply as follows: “Validation results revealed that the RMSE for the snow temperature profile and snow surface temperature were ~~comparable and~~ reasonable.” (**P31, L14**)

P519, L13: “to obtain an accurate SEB in the validation of the snow grain size calculated with the SMAP model,” → What is the main issue here - SEB or grain size? The two are connected, of course, through the impact of grain size on albedo.

Answer: As mentioned in our response to the general comment 2), we have dampen our argument regarding the 2LM method. In this section, our conclusion regarding the calculation method of latent heat flux is follows: “In order to confirm the validity of SEB characteristics during IOP, additional error analyses were conducted. During this process, it was turned out that the sign of latent heat fluxes from the 1LM and 2LM methods differed especially when the surface hoar was observed (3-5 July). The former showed negative, while the latter turned positive and designated the surface hoar formation. Therefore, the 2LM method calculated latent heat flux seemed to be plausible; however, uncertainty involved in the 2LM method was so large that we could not confirm its significance.” (**P33, L8**)

P519, L25: “we could confirm that the 2LM method was an effective way to obtain an accurate *H*L.” → I don't think you can be as definite as this without an independent measurement of HL for validation.

Answer: Thank you for this comment. As we responded to the previous comment, the

statement has been removed in the updated manuscript.

P527, L4: “observed temperature” → “observed surface temperature”

Answer: Corrected as suggested. (**Table 1**)

P529, L1: “IOP” → Give dates: 1-13 July 2012?

Answer: We have given the detail of IOP in the caption of Fig. 2. (**Fig. 2**)

P529, L2: “29 June 2012” → A bit confusing (sounds as if you are only presenting temperature measurements for 29 June). Why not say "...observed at a nominal height of 3 m above the snow surface"?

Answer: It is a nice suggestion. We have revised as suggested. (**Fig. 2**)

Reply to Reviewer #2

We are deeply grateful to the reviewer for taking the time to provide quite valuable comments and suggestions. Below we describe our responses (in black text) point-by-point to each comment (in blue text). In addition we indicate revisions in the updated manuscript by a yellow highlighter together with line numbers in the manuscript. Please also refer to the revised marked-up manuscript uploaded as a supplementary file. In the manuscript, change logs can be tracked.

General Comment:

It is a challenge to obtain high quality meteorological observations on the Greenland ice sheet, which the authors of this paper have achieved and should be congratulated for. Surface observations and modelling are used to characterize the surface energy balance and melt at a site in north-western Greenland, at an elevation of 1490 m a.s.l. The observations described are over a two week period, including the unprecedented event where widespread melt was observed over most of the Greenland ice sheet. The research is of interest as the atmospheric processes controlling this extreme melt event have not previously been described at this site. The measurements and modelling approach used in this research are described carefully and it is the view of this reviewer that the manuscript should be considered for publication. The comments provided below are intended to provide the authors with some feedback that they may wish to consider should the paper be considered for publication in The Cryosphere.

We would like to thank the reviewer for this encouraging evaluation. First, we summarize important revisions, which were conducted considering valuable comments from both reviewers, in the updated manuscript.

Major revisions:

It was pointed out that observed relative humidity with respect to water should be corrected after it is converted to relative humidity with respect to ice. We agree with this

point, and performed the correction that the reviewer suggested. Accordingly, input data for the SMAP model was modified and recalculations were performed. However, the results of this paper did not change significantly, because the values of relative humidity with respect to water and ice are almost the same under the condition that air temperature is around 0 °C. Related with this, scores indicating model performance, values of SEB fluxes, and some figures are changed slightly:

(**P17, L20**) 0.53 °C → 0.58 °C

(**P17, L23**) RMSE = 0.85 °C → RMSE = 0.94 °C

(**P17, L23**) ME = 0.55 °C → ME = 0.68 °C

(**P18, L15**) 0.16 → 0.17

(**P24, L25**) 15.2 → 15.3

(**P24, L25**) -13.2 → -18.0

(**P24, L25**) 17.8 → 7.2

(**P24, L26**) +31.0 → +25.2

(**P24, L27**) 102.5 → 96.7

(**P24, L28**) 55.0 → 49.1

(**P24, L28**) 24.9 to 79.9 → 20.1 to 69.2

(**P32, L28**) +31.0 → +25.2

Table1

Figures 6, 7, 8, 9, 10, 11, and 12

Both reviewers pointed out that error analysis investigating the significance of latent heat flux calculated from the 2LM method (air temperature, relative humidity, and wind speed at two profiles are employed to calculate turbulent heat flux at the surface) is necessary. It is because accuracy of air temperature, relative humidity, and wind speed sensors affect calculated latent heat flux with the 2LM method. In the original manuscript, we only investigated uncertainties induced by the snow surface roughness length for momentum. Now, we have completely understood and agreed with that it is insufficient, because it does not change the sign of latent heat flux but only modified its order. In addition, both reviewers commented that the turbulent heat fluxes in the presentation of SEB should be calculated in a consistent manner (only 1LM or 2LM).

Based on this consideration, we have reconstructed the paper especially after model evaluation section. Until Sect. 4, basic construction is as same as the original manuscript. After Sect. 5, we first present calculated SEB characteristics, where the turbulent heat fluxes are calculated employing only the 1LM method. Next, we discuss validity of the obtained SEB from various aspects in Sect. 6 "Discussion". In Sect. 6, we begin with investigating the effects of model setting on the SEB calculation (Sect. 6.1). In this subsection, we discussed impacts of the choices of snow surface roughness length and emissivity on the calculated SEB characteristics. The original discussion on the effects of snow surface roughness length has been reconstructed there (basic flow of discussion is as same as the original manuscript, but several corrections of sentences are performed). The motivation of investigating effects of emissivity on the SEB calculation was the comment by the reviewer regarding the validity of the choice of this value (comment on "9. P509, L18-23"). Finally, in Sect. 6.2 (reconstructed from the original Sect. 5 with some minor corrections of sentences), we discussed uncertainties in the 2LM method referring to valuable comments by both reviewers. In conclusion, we could only say that the 1LM method calculated latent heat flux could be underestimated and the 2LM method calculated latent heat flux seemed to be plausible; however, uncertainty involved in the 2LM method was so large that we could not confirm its significance, because gradients of air temperature, vapor pressure, and wind speed between two measurement heights (they were used for the 2LM calculation) were very small. Details of each relevant correction are explained in our responses to all related comments below. Technical corrections related to the reconstruction are as follows:

(**P18, L25**) Sect. 5 → Sect. 6.2

(**P19, L4**) Sect. 5 → Sect. 6.2

(**P24, L6**) Figure 11 → Figure 10

(**P24, L21**) Fig. 12 → Fig. 11

(**P24, L23**) Figure 12 → Figure 11

Figure 10a (**P21, L15**) → Figure 12a (**P28, L12**)

Figure 10c (**P22, L22**) → Figure 12b (**P29, L6**)

Fig. 10c (**P22, L25**) → Fig. 12b (**P29, L9**)

Fig. 10a (**P22, L28**) → Fig. 12a (**P29, L12**)
Fig. 10c (**P23, L10**) → Fig. 12b (**P29, L18**)

Minor revisions:

During revision process, we found a typo at the beginning of Sect. 2 in the original manuscript: "An automated weather station (AWS) was newly installed at site SIGMA-A on 29 ~~July~~ June 2012 (Aoki et al., 2014a)." It is corrected in the updated manuscript. (**P6, L14**)

Specific comments:

Please note that page number is referred to as (P) and line number is referred to as (L).

1. P496, L7-9 and L20-21: The abstract is well written and provides a clear framework of the paper. Two small comments that the authors may wish to consider. Firstly, the authors comment that 100 mm of rain fell during a "remarkable" melt event in the abstract. It would be of interest if the authors could provide more information in the site description (Section 2) about the long term climatology of the site, and whether "continuous" rainfall is an unusual event in summer at this location before making this statement in the abstract. Secondly, the assertion that two-level atmospheric profiles are "needed" to obtain realistic latent heat fluxes needs to be constrained if kept, to state that "in this study" it was found to be useful. Not enough evidence has been shown to suggest it should be widely adopted (further comments below).

Answer: We would like to thank the reviewer for these constructive comments. Related to the first comment, the Reviewer#1 also suggested we should give more information regarding the specificity of the meteorological condition during IOP in the context of long-term climatology. We agree with their point of view. As for the rainfall amount, we would like to answer in more detail at our feedback against the comment "6. P502, L1-12 and L22-25" below. Regarding the long term climatology of the site, our more detailed answer is presented at our correspondence against the comment "5. P500, L4-

24". Please consider our answer there.

For the question whether "continuous" rainfall is an unusual event in summer at this location or not?, we do not have any information. Although it is not a direct answer to the reviewer's comment, we would like to say that at least atmospheric condition was "unusual" at that time. To support this, we have added following discussion at Sect. 2.1: "Neff et al. (2014) examined synoptic-scale atmospheric conditions over the GrIS during July 2012 from various aspects and summarized notable features as follows: (1) warm air originating from a record North American heat wave (the North American drought of 2012 was the worst since 1895), (2) transitions in the Arctic Oscillation, (3) transport of water vapor via an Atmospheric River over the Atlantic to Greenland, and (4) the presence of warm ocean waters south of Greenland. Bonne et al. (2015) clearly showed that moist air mass was advected northward following a narrow band reaching southern Greenland and then it moved northward along the western Greenland coast around 9 July. Observed features of above mentioned meteorological properties during the IOP at the SIGMA-A site are consistent with these large-scale atmospheric conditions." (**P9, L1**). Here we intend to refer to "unusual condition" in the context of the long-term climatology by the following part of the revision above: "(1) warm air originating from a record North American heat wave (the North American drought of 2012 was the worst since 1895)".

Added references are:

Neff, W., Compo, G. P., Ralph, F. M., and Shupe, M. D.: Continental heat anomalies and the extreme melting of the Greenland ice surface in 2012 and 1889, J. Geophys. Res. Atmos., 119, 6520-6536, 10.1002/2014JD021470, 2014.

Bonne, J.-L., Steen-Larsen, H. C., Risi, C., Werner, M., Sodemann, H., Lacour, J.-L., Fettweis, X., Cesana, G., Delmotte, M., Cattani, O., Vallelonga, P., Kjær, H. A., Clerbaux, C., Sveinbjörnsdóttir, Á., E., and Masson-Delmotte, V.: The summer 2012 Greenland heat wave: In situ and remote sensing observations of water vapor isotopic composition during an atmospheric river event, J. Geophys. Res. Atmos., 120, 10.1002/2014JD022602, 2015.

The second point is quite important. As mentioned above, we have dampen our argument regarding the 2LM method, and related information have been removed from abstract. For more detail, please consider our answer to the comment "11. Section 5" below.

2. P498, L1-11: The authors may wish to consider providing an additional paragraph or replace paragraph two, which is quite general, with some of the key energy balance studies that have been carried out on the Greenland ice sheet margin, and/or in the interior. This might provide further context for readers about the expected radiative forcing due to clouds and the typical direction and magnitude of the turbulent heat fluxes. The controls on melt have been studied on the western margin of the Greenland ice sheet, so further justification and importance of the proposed research could be useful here.

Answer: Thank you very much for the constructive comment. We agree with the point that we should summarize key energy balance studies previously performed over the GrIS in the "Introduction" section. In this study, we focus on summer SEB characteristics at the SIGMA-A site. Thus, we have reviewed some important studies investigating summer (sometimes melting period) SEB features over GrIS, and added the following paragraph:

"Several attempts that focus on the summer GrIS SEB characteristics have been performed. Presented results show that the net shortwave radiant flux is the main contributor for the surface heating in general; however, detailed characteristics vary from place to place, and differ from year to year. Greuell and Konzelmann (1994) unveiled temporal changes in SEB at the ETH Camp (69°34'N, 49°18'W, 1155 m a.s.l.), west Greenland, during the 1990 summer (June, July, and August). During this summer, average net shortwave radiant flux (82 W m^{-2}) and sensible heat flux (34 W m^{-2}) acted to heat the surface, while average net longwave radiant flux (-54 W m^{-2}), latent heat flux (-28 W m^{-2}) played a role in cooling the surface. SEB characteristics during the 1991 summer at the same place was presented by Ohmura et al. (1994). According to

their results, the absolute values of each dominant SEB component averaged in this summer decreased obviously from the 1990 summer (net shortwave radiant flux was 65 W m^{-2}, net longwave radiant flux was -44 W m^{-2}, sensible heat flux was 16 W m^{-2}, and latent heat flux was -6 W m^{-2}, respectively). Summer SEB characteristics at the higher place on the GrIS was described by Cullen and Steffen (2001). They demonstrated that average turbulent (sensible and latent) heat fluxes at Summit (72°58'N, 38°51'W, 3203 m a.s.l.) during June 21 to July 6, 2000 were small (4 W m^{-2} and 3 W m^{-2}, respectively), while average net shortwave radiant flux (82 W m^{-2}) and net longwave radiant flux (-68 W m^{-2}) were comparable with previous results at ETH Camp. van den Broeke et al. (2011) presented long-term records of SEB at three AWSs situated along the K-transect, a stake array in southwest Greenland that extends from the ice margin to 1850 m a.s.l. They demonstrated that the temperature and moisture contrasts between ambient atmosphere and (melting) ice surface are less pronounced higher on the ice sheet, resulting in smaller summertime values of turbulent heat fluxes and net longwave radiant flux at the higher elevations." (**P4, L15**).

Here we have added the following four references related with this revision:

Cullen, N. J., and Steffen, K.: Unstable near-surface boundary conditions in summer on top of the Greenland Ice Sheet, Geophys. Res. Lett., 28, 4491-4493, doi: 10.1029/2001GL013417, 2001.

Ohmura, A., Konzelmann, T., Rotach, M., Forrer, J., Wild, M., Abe-Ouchi, A., and Toritani, H.: Energy balance for the Greenland ice sheet by observation and model computation, in: Snow and Ice Covers; Interaction With the Atmosphere and Ecosystems, Jones, H. G., Davies, T. D., Ohmura, A., Morris, E. M. (Eds.), IAHS, Gentbrugge, Belgium, 85-94, 1994.

van den Broeke, M. R., Smeets, C. J. P. P., and van de Wal, R. S. W.: The seasonal cycle and interannual variability of surface energy balance and melt in the ablation zone of the west Greenland ice sheet, The Cryosphere, 5, 377-390, doi:10.5194/tc-5-377-2011, 2011.

3. P500, L6-17: I am confident that the measurements are of a high quality but given the emphasis on determining gradients of wind speed, temperature and moisture in this paper I think it is necessary to clearly state the accuracy and/or precision of the RM Young (wind), HMP155 (temperature and relative humidity) instruments. Was a relative calibration of the instruments performed in the field or before or after deployment? If so, what was the precision of the instruments at the two heights? It would be useful to carefully demonstrate in this section that the instruments do allow gradients of wind speed, temperature and moisture to be resolved, before calculating turbulent heat fluxes from the two level method. Also, I would include the sampling rate of the instruments – averaging intervals are provided but sampling rates are not.

Answer: We completely agree with the reviewer's point of view that the accuracy of sensors affect turbulent heat fluxes from the 2LM method. In the revised manuscript, we decided to list up the absolute accuracy of each sensor as well as results of relative calibrations in newly reconstructed Sect. 6.2 as follows:

"In fact, numerical sensitivity studies with perturbed input parameters considering absolute accuracy of temperature, relative humidity, and wind speed sensors (±0.2 °C, ±2 %, and ±0.3 m s^{-1}, respectively) in the 2LM calculation modified the picture of calculated turbulent heat fluxes drastically in any calculations. Even when relative differences in the accuracy of two sensors at the lower and upper measurement heights were considered (according to our relative calibration of the instruments performed in advance, air temperature and wind speed sensors at two levels showed no significant difference; however, as for relative humidity, the upper sensor tended to be lower by 1.2 % compared to the lower sensor), differences in calculated latent heat flux with perturbed input parameters were quite large." (**P30, L8**)

The reviewer also noted the necessity of indicating sampling rate. Related to this, the original description regarding the data storing procedure ("Measured data were averaged every 1 min and stored in a data logger (CR1000, Campbell, USA)." P500, L14 in the original manuscript) was not accurate. Now we have revised as follows:

"Measured data were sampled and stored in a data logger (CR1000, Campbell, USA)

every 1 min." (**P7, L19**).

4. P498, L1-11: It is common to apply a procedure to recalculate relative humidity data to account for saturation with respect to ice rather than liquid water (e.g. Box and Steffen, 2001). Was this correction attempted? If not, the authors may wish to comment on whether they think such a correction would or wouldn't have an impact on the absolute humidity values used to calculate the latent heat flux.

Answer: Thank you very much for the very important information. We investigated related previous studies (including Box and Steffen (2001)) again and recognized that it is quite popular to correct relative humidity with respect to ice using the method presented by Anderson (1994), which is employed by Box and Steffen (2001). In the revised manuscript, we have performed the correction against relative humidity with respect to ice converted from observed relative humidity with respect to water. It is now stated in the revised version as follows: "As for relative humidity with respect to water, we converted it into relative humidity with respect ice when air temperature was below 0 °C, and performed the correction presented by Anderson (1994)." (**P7, L9**).

It means that the input data for the SMAP model were modified, and we performed recalculation accordingly as mentioned above. However, relative humidities with respect to ice and water are almost on the same level under the condition that air temperature is near 0 °C, and main conclusions of this study is not affected by this modification.

We have added the following reference related with this revision:

Anderson, P. S.: A method for rescaling humidity sensors at temperatures well below freezing, J. Atmos. Oceanic Technol., 11, 1388-1391, doi:10.1175/1520-0426(1994)011<1388:AMFRHS>2.0.CO;2, 1994.

5. P500, L4-24: The description of the meteorological conditions in this section is of interest, but before presenting data from the measurement period it might be of useful to have further context about the background long-term climatological conditions at the site (see point 1). Prior to the "exceptional" melt event, were conditions typical for this elevation and latitude? A climatological context for the measurements would provide a broader context for readers.

Answer: It is a nice suggestion. However, because the SIGMA-A AWS is a newly installed one, we estimated "possible" climate condition at the site referring two GC-Net AWS data (Humboldt and GITS) (Steffen and Box., 2001) located in the northwest GrIS at the beginning of Sect. 2 as follows:

"In the northwest GrIS, two GC-Net AWS sites exist (Steffen and Box., 2001); one is the Humboldt site (78°32'N, 56°50'W, 1995 m a.s.l.) and the other is the GITS site (77°08'N, 61°02'W, 1887 m a.s.l.). Steffen and Box (2001) presented monthly mean temperature at these stations and also demonstrated that the mean temperature lapse rate over GrIS in summer to be 0.4°C per 100 m. These information allow us to estimate possible average near-surface air temperature during July at the SIGMA-A site, and it was around -6.5°C." (**P6, L15**)

These discussion has allowed us to give the wider interpretation of measured air temperature at the SIGMA-A site (Sect. 2.1):

"Figure 2 presents time series of meteorological conditions measured with the AWS during the IOP. Until 9 July, air temperature at 3.0 m above the surface was already high and often exceeded 0 °C in the daytime. The time interval from 10 July until the end of the IOP coincided with the record near-surface melt event period reported by Nghiem et al. (2012); during that time air temperature increased slightly and remained above 0 °C, which is much larger than the estimated possible average air temperature at the SIGMA-A site: -6.5 °C (Sect. 2), continuously (Fig. 2a)." (**P8, L10**)

Added reference:

Steffen, K., and Box, J.: Surface climatology of the Greenland Ice Sheet: Greenland Climate Network 1995-1999, J. Geophys. Res., 106(D24), 33951--33964, doi: 10.1029/2001JD900161, 2001.

6. P502, L1-12 and L22-25: The authors should consider providing a precipitation normal for the site, which may help explain the discrepancy between the reanalysis and bucket rain gauge. The near surface layer (NSL) was 88 cm – is this the accumulation over the last 12-months? This needs clarification. Also, it is this referee's understanding that snow temperatures obtained from snow pit measurements were used to initialize and then validate SMAP. It appears that observations were taken on 12 days (June 30 to 13 July, except for 11 and 12 July). Are the authors confident that the RMSE calculated in Table 1 has sufficient samples to be meaningful? It might be useful to confirm to readers how many in situ measurements were available for model comparison.

Answer: Firstly, we have mentioned a precipitation normal in SIGMA-A referring Ohmura and Reeh (1991)'s result as follows: "According to Ohmura and Reeh (1991), annual total precipitation near the SIGMA-A site is extrapolated to be around 200 – 300 mm w.e. The estimated total precipitation during this event can account for more than 30 – 50 % of the annual total precipitation." (**P10, L4**)

Regarding the next comment, it has not been determined whether the NSL is the latest annual layer or not, because of the lack of justification. Further information from chemical analysis, for example, would be necessary (this attempt is ongoing). In the revised manuscript, we have indicated it as follows: "At present, the NSL has not been determined to be the latest annual layer, because the lack of justification." (**P10, L18**)

The last question is related to the significance of RMSE and ME of calculated snow temperature. During IOP, total 221 profiles (after rejecting strange data) were available for the validation of snow temperature profile calculated by the SMAP model. We believe it is sufficient for this kind of assessment. In the revised manuscript, it is indicated as follows: "In this comparison, total 221 profiles (after rejecting strange data) were available." (**P11, L5**)

Added reference:

Ohmura, A., and Reeh, N.: New precipitation and accumulation maps for Greenland, J. Glaciol., 37, 140-148, 1991.

7. P506, L1-2: The significance of surface roughness lengths is discussed at length in this paper in relation to their control on the turbulent heat fluxes. It appears that the stability functions are calculated using a Richardson Number, and that an upper bound of 0.1 was set. How influential was this decision compared to changing the magnitude of the surface roughness lengths?

Answer: The upper bound of Richardson number (0.1) ensures small but non-zero exchange of turbulent heat flux even under strongly stable condition. During IOP, low wind speed (lower than 1.0 m s^{-1}) were rarely observed at the SIGMA-A site. As a result, such a strongly stable condition was not observed on-site, and we could not confirm the effect of this setting. It is stated at the end of Sect. 3.1 of the updated manuscript as follows: "During IOP, low wind speed were rarely observed at the SIGMA-A site as mentioned in Sect. 2.1. As a result, preliminary numerical simulation revealed that the impact of the upper bound was not clear during IOP; however, it is still set in this study." (**P14, L1**)

8. P508, L21-23: How was the NSL simulated by the model adjusted to the measured depth? It is not clear how this was done, and a comment on the reasons for any discrepancy might be useful to readers.

Answer: In this procedure, model simulated NSL thickness (the SMAP model tended to underestimate by -2.0 cm, which may be sufficiently enough, during IOP compared to the snow pit measurements) was simply stretched to adjust the snow-pit measurements. Here, model simulated internal properties were not modified at all, implying that the mass in the NSL is not conserved "only during this process"; however, this is completely a post-process management and does not affect the model simulation itself.

The small error of -2.0 cm makes it difficult to look at meaningful possible causes of the discrepancy. Thus, we have revised as follows: "When a measured snow temperature profile was compared against simulation results, the depth of the NSL simulated by the model (the SMAP model tended to underestimate the NSL's depth by -2.0 cm compared to the snow pit measurements during the IOP) was adjusted to the measured depth as a post-process, where model simulated internal properties were not modified at all." (**P16, L19**)

9. P509, L18-23: The emissivity chosen was 0.98, which is lower than the values chosen in other studies over the Greenland ice sheet, where unity has been assumed (e.g. van den Broeke et al., 2008). Was the same emissivity used in the model? If the measured snow surface temperature had been calculated assuming an emissivity of 1 would the offset between SMAP and observed surface temperature would have been larger? Bottom line: are the authors satisfied that the emissivity chosen is not affecting the calculation of the latent heat flux using the 1D method? Could this help explain the failure to detect deposition events (Section 4.3)? Also, Figure 7 appears to indicate that after 10 July both model and measured snow temperatures were constantly at melting point – is this the case?, the lines are hard to detect.

Answer: First of all, we should comment that the same emissivity (0.98) was used in the process of obtaining observed snow surface temperature, as well as the SMAP model calculation. In order not to cause misunderstanding to readers, we have added an explanation that emissivity of 0.98 was employed by the SMAP model in the model description section as follows: "In addition, the emissivity of the snow surface ε was assumed to be 0.98 (Armstrong and Brun, 2008; van As, 2011) throughout this study." (**P15, L22**). Related with this revision, we have removed the original description introducing emissivity in Sect. 4. In the added description highlighted above, we have cited van As (2011) who employed the value of 0.98 in the GrIS. Basically, we think that there are no good grounds for both values of emissivity (0.98 or 1), which may cause uncertainties in SEB calculations. Therefore, we discussed uncertainties induced by the choice of this value in the newly added discussion section (Sect. 6.1) as follows: "Secondly, we investigated effects of ε_s introduced in Sect. 3.3 on SEB calculations. In this sensitivity test, ε_s was set to be 1.0 and surface temperature (to be input to the

SMAP model) was calculated only from observed $L^{\uparrow}$. The result indicated that mean differences of turbulent heat fluxes against the original SEB calculation were 1.1 w m^{-2} and 0.9 W m^{-2} for H_S and H_L, respectively. This result implies that the sensitivity of SEB calculation to the choice of ε_s is small, and SEB characteristics during IOP at the SIGMA-A site presented in Sect. 5 is still valid. van As (2011) also performed this type of sensitivity test and demonstrated ε_s 's small impact on the SEB calculation." (**P26, L26**)

As for Fig. 7, its presentation has been modified.

10. P511, L16-18 and P512, L6-12: The measurement and modelling of near-infrared radiation is very interesting and is often not explicitly treated in energy balance modelling studies. The variability of the surface albedo around 4 July and 10 July is quite significant, and it is impressive how model and measurements agree (Figure 9). The explanation for this variability is linked to near-infrared, UV-visible and diffuse fractions of downward shortwave radiation. The authors could consider placing a little more emphasis on this finding, as it is an interesting result. A more detailed explanation about the physical processes controlling changes in snow albedo on the temporal scale shown in Figure 9 would be insightful for readers.

Answer: We would like to thank this encouraging comment. As a matter of fact, the SMAP model owes much of the "impressive" result to the PBSAM developed by Aoki et al. (2011) that explicitly treats the physical processes both in the atmosphere and the snowpack, which are explained in the manuscript. We considered what should be specially mentioned more, and decided to discuss as follows: "Therefore, once the SMAP model or the PBSAM are coupled with atmospheric models, it is necessary for such host atmospheric models to simulate the presence or absence of cloud realistically. King et al. (2014) also argued that efforts to improve model simulations of surface energy balance and melt in the polar region should concentrate initially on reducing biases in modeled shortwave and longwave radiation, which are caused by deficiencies in the representation of cloud properties." (**P19, L18**). It is also stated in the conclusion section as "These physical processes are explicitly taken into account by the PBSAM, an important component of the SMAP model, highlighting that an advantage of

PBSAM." (**P32, L1)**, and in the abstract as "Above all, the fact that the SMAP model successfully reproduced frequently observed rapid increases in snow albedo under cloudy-conditions highlights the advantage of the Physically Based Snow Albedo Model (PBSAM) incorporated in the SMAP model." (**Abstract**).

Added reference:

King, J. C., Gadian, A., Kirchgaessner, A., Kuipers Munneke, P., Lachlan-Cope, T. A., Orr, A., Reijmer, C., van den Broeke, M. R., van Wessem, J. M., and Weeks, M.: Validation of the summertime surface energy budget of Larsen C Ice Shelf (Antarctica) as represented in three high-resolution atmospheric models. J. Geophys. Res. Atmos., 120, 1335-1347, doi:10.1002/2014JD022604, 2015.

11. Section 5: To improve this analysis it might be useful for the authors to present temperature and moisture gradients (surface and two levels in the atmosphere) to determine from the outset what the fundamental difference is between comparing surface atmosphere and atmosphere at two levels. This could also aid the authors in addressing point 3 – the uncertainty of the instruments. In this context it should be noted that Box and Steffen (2001) had good agreement in determining the sign and magnitude of the latent heat flux using the 1D and 2D methods at low elevations on the Greenland ice sheet but greater uncertainty existed at higher elevations (sign often changed – see Table 6; for further discussion see Cullen et al., 2014). Though the authors focus on changing the magnitude of the surface roughness values (pg. 514), this should only have the effect of increasing or decreasing the magnitude of the latent heat flux, not the sign (direction), which appears to be the issue (not resolving deposition events). The discussion on pg. 515 could be re-focused if the atmospheric controls on the gradients of moisture and temperature are resolved more clearly.

Answer: Very insightful comments that we should consider without fail. In the reconstructed manuscript, discussion on disparities between the 1LM and 2LM methods are placed in Sect. 6.2, while sensitivity studies investigating effects of the snow surface roughness length was conducted in Sect. 6.1 as mentioned above.

First, we have mentioned important results by Box and Steffen (2001) and Cullen et al. (2014), which we agree with that we should refer to, in the third paragraph of Sect. 6.2 (**P28, L12~**), where we compared latent heat fluxes from the 1LM and 2LM methods at the SIGMA-A site during the period:

"Obviously, the result indicated that the latent heat flux from OBS_1LM was almost compatible with the heat flux from SMAP_1LM, implying that the OBS_1LM is also likely to underestimate the latent heat flux. Comparison between OBS_2LM and OBS_1LM shows that the former obviously tends to be higher than the latter, and sometimes the signs of the fluxes are different. According to previous studies (Box and Steffen, 2001; Cullen et al., 2014), the sign and magnitude of the latent heat fluxes from the 1LM and 2LM methods agree reasonably at low elevations on the GrIS, whereas they often differ from each other at the higher elevations. Measurements conducted previously in the northwest GrIS (the Humboldt and GITS sites) showed that the net annual sublimation from the 1LM and 2LM methods did not agree sufficiently at both sites (Box and Steffen, 2001). In the former site, the sign was contrasting, while the magnitude was remarkably different at the latter site." (**P28, L15**)

In the next (fourth) paragraph of Sect. 6.2 (**P29, L1**), we demonstrated that the SMAP model forced by two level measurements succeeded in reproducing the surface hoar, which discussion is basically as same as the original manuscript. However, several minor revisions were performed in order to maintain consistency in the manuscript.

Then, in the last paragraph of Sect. 6.2, we calculated wind speed, temperature, and moisture gradients (surface and two levels in the atmosphere) as suggested. Obtained gradients for wind speed, air temperature, and vapor pressure between the surface and the lower measurement height (positive downward) were 1.6 s^{-1}, 0.3 °C m^{-1}, and -0.15 hPa m^{-1}, respectively during the IOP. However, those values between the lower and upper measurement heights were nearly 0, except for the case of wind speed: 0.2 s^{-1}. If we focused on the period from 00:10 to 00:20 UTC on 4 July when SMAP_2LM detected the surface hoar, we found that vapor pressure gradients showed opposite signs: -0.13 hPa m^{-1} for the 1LM method and 0.01 hPa m^{-1} for the 2LM method,

respectively. This result explains why the 1LM method failed to detect the surface hoar, whereas the 2LM method succeeded in that. However, those gradients between the lower and upper sensors are too low to detect significant uncertainties caused by the sensor accuracy. The accuracy of each sensor and results from relative calibration between the lower and upper sensors are presented here. As a result, we decided to discuss the uncertainties of the 2LM method as follows:

"According to Box and Steffen (2001), the uncertainty of the 2LM method increases as the temperature, humidity, and wind speed differences between two measurement heights decrease. These motivated us to investigate the significance of the 2LM method calculated latent heat flux during IOP. In this inquiry, gradients (positive downward) of wind speed, temperature, and vapor pressure between the surface and the lower measurement height, as well as those between the lower and upper measurement heights were investigated at first. Averaged gradients between the surface and the lower measurement height during the IOP were 1.6 s^{-1}, 0.3 °C m^{-1}, and -0.15 hPa m^{-1}, respectively. The value for vapor pressure is very close to that obtained at Summit during 2000–2002 reported by Cullen et al. (2014). On the other hand, averaged gradients between the lower and upper measurement heights were nearly 0, except for the case of wind speed: 0.2 s^{-1}. Focusing on the period from 00:10 to 00:20 UTC on 4 July when SMAP_2LM detected the surface hoar, vapor pressure gradients showed opposite signs: -0.13 hPa m^{-1} for the 1LM method and 0.01 hPa m^{-1} for the 2LM method, respectively. Although this result explains the reason why only the 2LM method succeeded in the surface hoar detection, the latter value is still very small. These make it difficult to assess uncertainties of the 2LM method caused by each sensor as expected. In fact, numerical sensitivity studies with perturbed input parameters considering absolute accuracy of temperature, relative humidity, and wind speed sensors (±0.2 °C, ±2 %, and ±0.3 m s^{-1}, respectively) in the 2LM calculation modified the picture of calculated turbulent heat fluxes drastically in any calculations. Even when relative differences in the accuracy of two sensors at the lower and upper measurement heights were considered (according to our relative calibration of the instruments performed in advance, air temperature and wind speed sensors at two levels showed no significant difference; however, as for relative humidity, the upper sensor tended to be lower by 1.2 % compared to the lower sensor), differences in calculated latent heat flux with perturbed input parameters were quite large. Therefore, we should conclude that underestimation of the latent heat flux calculated with the 1LM method could be plausible, although the exact order of underestimation was quite hard to detect during

this study period." (**P29, L21**)

We have added following references in the updated manuscript:

Cullen, N. J., Mölg, T., Conway, J., and Steffen, K.: Assessing the role of sublimation in the dry snow zone of the Greenland ice sheet in a warming world, J. Geophys. Res. Atmos., 119, 6563–6577, doi:10.1002/2014JD021557, 2014.

12. P516, L1-9: Please clarify how the energy available for melt is treated in the model and in equation 6. In line with point 11 it would seem more logical to calculate both the turbulent heat fluxes in a consistent manner (either 1D or 2D but not a mixture of the two).

Answer: For the first point, we have mentioned the detail as follows: "The snow surface is heated when the flux is positive and surface melt is occurred if the surface temperature is 0 °C, whereas it is cooled if the flux is negative." (**P23, L26**)

As for the next point, we have unified the calculation method for turbulent heat flux (only the 1LM method was used) as explained at the beginning of this response. Related with this, the statement: "However, based on the discussion in Sect. 5, only *H*L was calculated by using the 2LM approach." has been removed. (**P24, L4**)

13. P517, L7-29: The energy balance during melting resembles what has been observed in the ablation areas of Norway's glaciers, and other mid-latitude glaciers (e.g. Giesen et al., 2009; 2014). The authors might wish to make this linkage rather than just referring to the Bennartz et al. (2013) publication.

Answer: Thank you very much for this interesting information. We checked these references, and decided to cite the information in this section as follows: "These values, calculated during Period-1, are almost equal to the surface fluxes from June to August averaged during the summers of 2000-2011 over the GrIS accumulation area based on the MAR regional climate model (Fettweis et al., 2011) and MODIS data presented by

Box et al. (2012). On the other hand, the SEB characteristics during Period-2 (signs and orders) resemble those obtained at Langfjordjøkelen, Norway (Giesen et al., 2014). (**P25, L3**)

14. P518-520: The statement that the 2D method is "preferable" over the 1D method to calculate the latent heat flux (P519, L26-29, P520, L1-2) requires more evidence before it can be suggested for use more broadly (see point 1). As indicated in point 11, an analysis of temperature and moisture gradients might be a useful way to clarify to readers why the 1D method is not reproducing deposition events.

Answer: Based on our response against the comment 11, we have reconstructed the conclusion section. In the revised manuscript, we have removed the last paragraph of the "Conclusion" section in the original manuscript, and we only mentioned as follows "In order to confirm the validity of SEB characteristics during IOP, additional error analyses were conducted. During this process, it was turned out that the sign of latent heat fluxes from the 1LM and 2LM methods differed especially when the surface hoar was observed (3-5 July). The former showed negative, while the latter turned positive and designated the surface hoar formation. Therefore, the 2LM method calculated latent heat flux seemed to be plausible; however, uncertainty involved in the 2LM method was so large that we could not confirm its significance." (**P33, L8**)

Technical corrections

P498, L5-L6: present tense could be used – "these fluxes are defined to be positive when they are directed

Answer: Corrected as suggested (**P4, L8**).

P501, L1: these data could be used rather than "this" data

Answer: Revised as suggested (**P8, L7**).

P507, L8: we calculated the temporal evolution – add "the"

Answer: We have added "the" as suggested (**P15, L7**)

P507, L12: resolution for an Arctic snowpack – add "an"

Answer: Revised as suggested (**P15, L11**).

References

Bennartz, R., M.D. Shupe, D.D. Turner, V.P. Walden, K. Steffen, C.J. Cox, M.S. Kulie, N.B. Miller and C. Pettersen (2013), July 2012 Greenland melt extent enhanced by low-level liquid clouds, Nature, 496, 83–86, doi:10.1038/nature12002.

Box, J.E., and K. Steffen (2001), Sublimation on the Greenland ice sheet, J. Geophys. Res., 106(D24), 33,965-33,982.

Cullen, N.J., T. Mölg, J. Conway, and K. Steffen (2014), Assessing the role of sublimation in the dry snow zone of the Greenland ice sheet in a warming world, J. Geophys. Res., 119, 6563–6577, doi:10.1002/2014JD021557.

Giesen R.H., L.M. Andreassen, J. Oerlemans and M.R. van den Broeke (2014), Surface energy balance in the ablation zone of Langfjordjøkelen, an arctic, maritime glacier in northern Norway, J. Glaciol., 60, 57-70, doi: 10.3189/2014JoG13J063.

Giesen R.H., L.M. Andreassen, M.R. van den Broeke, and J. Oerlemans (2009),

Comparison of the meteorology and surface energy balance at Storbreen and Midtdalsbreen, two glaciers in southern Norway, Cryosphere, 3(1), 57–74, doi:10.5194/tc-3-57-2009.

van den Broeke, M.R., C.J.P.P. Smeets, and R.S.W. van de Wal (2011), The seasonal cycle and interannual variability of surface energy balance and melt in the ablation zone of the west Greenland ice sheet, The Cryosphere, 5(2), 377–390 (doi:10.5194/tc-5-377-2011)

van den Broeke, M.R., P. Smeets, and J. Ettema (2008), Surface layer climate and turbulent exchange in the ablation zone of the west Greenland ice sheet, Int. J. Climatol., 29, 2309–2323, doi:10.1002/joc.1815.

Manuscript prepared for The Cryosphere Discuss.
with version 2014/09/16 7.15 Copernicus papers of the LaTeX class copernicus.cls.
Date: 15 April 2015

Numerical simulation of extreme snow melt observed at the SIGMA-A site, northwest Greenland, during summer 2012

M. Niwano[1], T. Aoki[1], S. Matoba[2], S. Yamaguchi[3], T. Tanikawa[4], K. Kuchiki[1], and H. Motoyama[5]

[1]Meteorological Research Institute, Japan Meteorological Agency, Tsukuba, Japan
[2]Institute of Low Temperature Science, Hokkaido University, Sapporo, Japan
[3]Snow and Ice Research Center, National Research Institute for Earth Science and Disaster Prevention, Nagaoka, Japan
[4]Earth Observation Research Center, Japan Aerospace Exploration Agency, Tsukuba, Japan
[5]National Institute of Polar Research, Tachikawa, Japan

Correspondence to: M. Niwano (mniwano@mri-jma.go.jp)

Abstract

The surface energy balance (SEB) from 30 June to 14 July 2012 at site SIGMA (Snow Impurity and Glacial Microbe effects on abrupt warming in the Arctic)-A, (78°03′ N, 67°38′ W; 1490 m a.s.l.) on the northwest Greenland Ice Sheet (GrIS) was investigated by using in situ atmospheric and snow measurements, as well as numerical modeling with a one-dimensional, multi-layered, physical snowpack model called SMAP (Snow Metamorphism and Albedo Process). At SIGMA-A, remarkable near-surface snowmelt and continuous heavy rainfall (accumulated precipitation between 10 and 14 July was estimated to be 100 mm) were observed after 10 July 2012. Application of the SMAP model to the GrIS snowpack was evaluated based on the snow temperature profile, snow surface temperature, surface snow grain size, and shortwave albedo, all of which the model simulated reasonably well. ~~However, comparison of the SMAP-calculated surface snow grain size with in situ measurements during the period when surface hoar with small grain size was observed on-site revealed that it was necessary to input air temperature, relative humidity, and wind speed data from two heights to simulate the latent heat flux into the snow surface and subsequent surface hoar formation. The calculated latent heat flux was always directed away from the surface if data from only one height were input to the SMAP model , even if the value for roughness length of momentum was perturbed between the possible maximum and minimum values in numerical sensitivity tests. This result highlights the need to use two-level atmospheric profiles to obtain realistic latent heat flux~~Above all, the fact that the SMAP model successfully reproduced frequently observed rapid increases in snow albedo under cloudy-conditions highlights the advantage of the Physically Based Snow Albedo Model (PBSAM) incorporated in the SMAP model. Using such ~~profiles, we calculated~~ data and model, we estimated the SEB at SIGMA-A from 30 June to 14 July 2012. Radiation-related fluxes were obtained from in situ measurements, whereas other fluxes were calculated with the SMAP model. By examining the components of the SEB, we determined that low-level clouds accompanied by a significant temperature increase played an impor-

tant role in the melt event observed at SIGMA-A. These conditions induced a remarkable surface heating via cloud radiative forcing in the polar region.

1 Introduction

Snow and ice on the Greenland ice sheet (GrIS) experienced a record near-surface melt extent in summer 2012 (Nghiem et al., 2012; Tedesco et al., 2013; Hall et al., 2013; Hanna et al., 2014; Bennartz et al., 2013). The physical conditions of the atmosphere and the snow (as well as ice) surface during summer 2012 have been gradually clarified. The most notable feature of the event is that the extent of surface melt was the largest in the satellite era (March 2000 to the present). According to several studies that used satellite data (Nghiem et al., 2012; Tedesco et al., 2013; Hall et al., 2013), at least 95 % of the entire surface of the GrIS melted during the period 30 June to 14 July 2012. At present, it is hypothesized that a significant temperature increase over the GrIS may have been a major cause of the record near-surface melt event. Hall et al. (2013) examined the ice surface temperature (IST) of the GrIS derived from the Moderate-resolution Imaging Spectroradiometer (MODIS) and concluded that the 2012 summer was the warmest (IST: $-6.38 \pm 3.98\,^{\circ}\mathrm{C}$) in the MODIS record. Bennartz et al. (2013) have demonstrated that low-level clouds consisting of liquid-water droplets played a key part in the melt event by increasing near-surface temperature via radiative effects. Nghiem et al. (2012) pointed out the existence of an anomalous ridge of warm air that could be identified by a 500 hPa height anomaly, and they concluded that the ridge acted as a strong heat dome that became stagnant over the GrIS during the period. Hanna et al. (2014) concluded that the extreme melt was forced mainly by atmospheric conditions linked with changes in the summer North Atlantic Oscillation (NAO), Greenland Blocking Index (GBI), and polar jet stream. The combination of these conditions favored southerly warm air advection along the western coast. According to Fettweis et al. (2013), the frequency of occurrence of anticyclones centered over the GrIS at the surface and at 500 hPa has doubled since the end of the 1990s. They associated this increased frequency with an increase of negative phases of the NAO, which induce more frequent southerly

warm air advection along the western Greenland coast and over the neighboring Canadian Arctic Archipelago.

However, a ~~temperature increase is unlikely to be the only cause of surface melt , because surface melt~~ temperature increase cannot induce surface melt if the surface temperature, which is physically controlled by the surface energy balance (SEB), is below 0 °C. The SEB is equal to the sum of the net shortwave radiant flux, net longwave radiant flux, sensible heat flux, latent heat flux, heat supply by rainfall, and subsurface conductive heat flux (Armstrong and Brun, 2008). In this study, these fluxes ~~were~~ are defined to be positive when they ~~were~~ are directed towards the snow surface, and a positive sum of these fluxes (net energy flux) induces surface melt only if the surface temperature equals 0 °C. A temperature increase raises the net energy flux mainly by affecting the sensible heat flux, although other energy fluxes, especially net longwave radiant flux, can of course be affected by a temperature increase. Therefore, it is necessary to pay close attention to other fluxes in addition to the sensible heat flux when surface melt is investigated.

Several attempts that focus on the summer GrIS SEB characteristics have been performed. Presented results show that the net shortwave radiant flux is the main contributor for the surface heating in general; however, detailed characteristics vary from place to place, and differ from year to year. Greuell and Konzelmann (1994) unveiled temporal changes in SEB at the ETH Camp (69°34′ N, 49°18′ W, 1155 m a.s.l.), west Greenland, during the 1990 summer (June, July, and August). During this summer, average net shortwave radiant flux (82 W m^{-2}) and sensible heat flux (34 W m^{-2}) acted to heat the surface, while average net longwave radiant flux (-54 W m^{-2}), latent heat flux (-28 W m^{-2}) played a role in cooling the surface. SEB characteristics during the 1991 summer at the same place was presented by Ohmura et al. (1994). According to their results, the absolute values of each dominant SEB component averaged in this summer decreased obviously from the 1990 summer (net shortwave radiant flux was 65 W m^{-2}, net longwave radiant flux was -44 W m^{-2}, sensible heat flux were 16 W m^{-2}, and latent heat flux was -6 W m^{-2}, respectively). Summer SEB characteristics at the higher place on the GrIS was described by Cullen and Steffen (2001). They demonstrated that average turbulent (sensible and

latent) heat fluxes at Summit (72°58′ N, 38°51′ W, 3203 m a.s.l.) during June 21 to July 6, 2000 was small (4 W m^{-2} and 3 W m^{-2}, respectively), while average net shortwave radiant flux (82 W m^{-2}) and net longwave radiant flux ($-$68 W m^{-2}) were comparable with previous results at ETH Camp. van den Broeke et al. (2011) presented long-term records of SEB at three AWSs situated along the K-transect, a stake array in southwest Greenland that extends from the ice margin to 1850 m a.s.l. They demonstrated that the temperature and moisture contrasts between ambient atmosphere and (melting) ice surface are less pronounced higher on the ice sheet, resulting in smaller summertime values of turbulent heat fluxes and net longwave radiant flux at the higher elevations.

In the present study, our goal was to understand the record near-surface melt event that occurred over the GrIS in 2012 by investigating snow-atmosphere interactions from the standpoint of the SEB. For this purpose, we employed data obtained from in situ measurements made at a site named SIGMA (Snow Impurity and Glacial Microbe effects on abrupt warming in the Arctic)-A (Aoki et al., 2014a) in northwest Greenland during the 2012 summer intensive observation period (30 June to 14 July) (hereafter: IOP). During the latter half of the IOP, which coincided with the period of the record near-surface melt event reported by Nghiem et al. (2012), we observed remarkable melting of the near-surface snowpack and encountered continuous rainfall (Aoki et al., 2014b; Yamaguchi et al., 2014). In the process of calculating the SEB, radiation-related terms could be determined from in situ measurements (described in Sect. 2); however, the sensible heat flux, latent heat flux, and heat supply by rainfall, which were not measured directly at the SIGMA-A site, had to be calculated in some way. In this study, we therefore calculated these fluxes by using the physical snowpack model SMAP (Snow Metamorphism and Albedo Process), which was originally developed and evaluated against seasonal snowpack (Niwano et al., 2012, 2014). Because this study was the first attempt to apply the SMAP model in a polar region, we carried out a preliminary examination of various aspects of the capacity of the SMAP model. This model validation study was expected to increase the reliability both of the SMAP model itself and of the Meteorological Research Institute Earth System Model version1 (MRI-ESM1) (Yukimoto

et al., 2011), in which the SMAP model is used to calculate energy exchanges between the snow surface and atmosphere in the global cryosphere.

We begin part 2 of this paper by presenting an outline of our in situ measurements conducted at SIGMA-A during summer 2012. Then we describe the modification of the SMAP model that enabled its use to simulate polar conditions. We verified the accuracy of the model with respect to the snow temperature profile, snow surface temperature, surface optically equivalent snow grain radius, and shortwave albedo. Finally, we used the SMAP model to explore the SEB during the IOP at the SIGMA-A site by diagnosing the turbulent heat fluxes and heat supplied by rainfall.

2 Field measurements at the SIGMA-A site

In this section we report the in situ data acquired during the IOP at site SIGMA-A (78°03′ N, 67°38′ W, 1490 m a.s.l.) (Aoki et al., 2014a) in northwest Greenland (Fig. 1), and we report the observed meteorological and snow conditions. An automated weather station (AWS) was newly installed at site SIGMA-A on 29 ~~July~~June 2012 (Aoki et al., 2014a). In the northwest GrIS, two GC-Net AWS sites exist (Steffen and Box., 2001); one is the Humboldt site (78°32′ N, 56°50′ W, 1995 m a.s.l.) and the other is the GITS site (77°08′ N, 61°02′ W, 1887 m a.s.l.). Steffen and Box (2001) presented monthly mean temperature at these stations and also demonstrated that the mean temperature lapse rate over GrIS in summer to be 0.4 °C per 100 m. These information allow us to estimate possible average near-surface air temperature during July at the SIGMA-A site, and it was around −6.5 °C. This region of the northwestern GrIS is now being carefully monitored, because since around late 2005 the ice loss over southern portions of the GrIS has been spreading rapidly northward along the northwest coast (Khan et al., 2010). Dates and times throughout this paper are expressed in terms of the universal time clock (UTC); the difference between local time (LT) at site SIGMA-A and UTC is −2 h.

2.1 Meteorological observations

The AWS measured air temperature and relative humidity with respect to water with a humidity and temperature probe (HMP155, Vaisala, Finland) protected from direct solar irradiance by a naturally aspirated, 14-plate Gill radiation shield (41005, Young, USA) at 3.0 and 6.0 m above the snow surface on 29 June. According to van den Broeke et al. (2009), radiation errors in the unventilated air temperature measurement can be up to 3 °C under conditions of low wind speed and high insolation. However, no corrections were made to measured air temperature in the present study, because low wind speeds ($< 1.0\,\mathrm{m\,s^{-1}}$) were rarely observed at SIGMA-A during IOP as noted later in this section. As for relative humidity with respect to water, we converted it into relative humidity with respect ice when air temperature was below 0 °C, and performed the correction presented by Anderson (1994). The AWS also measured wind speed and direction with a wind monitor (05103, Young, USA) at 3.0 and 6.0 m above the surface. The AWS was also equipped with a digital barometer (PTB210, Vaisala, Finland), and an ultrasonic distance sensor (SR50, Campbell, USA) for snow depth monitoring. We used a net radiometer (CNR4, Kipp & Zonen, Netherlands) to measure downward and upward shortwave (wavelength $\lambda = 0.305$–$2.8\,\mu\mathrm{m}$) and longwave ($\lambda = 4.5$–$42\,\mu\mathrm{m}$) radiant fluxes. Downward and upward near-infrared ($\lambda = 0.715$–$2.8\,\mu\mathrm{m}$) radiant fluxes were observed by pyranometers (CMP6, Kipp & Zonen, Netherlands) with RG715 cut-off filter domes. Measured data were ~~averaged~~sampled~~every 1 min~~ and stored in a data logger (CR1000, Campbell, USA) every 1 min. Aoki et al. (2014a) have provided a more detailed description of the AWS. In the present study, we used 5 min average values of AWS data, but to highlight important temporal evolution, the SEB data reported after Sect. 5 are 1 h averages.

In addition to the automatic measurements, we performed manual spectral albedo measurements using a field spectroradiometer (FieldSpec 3, Analytical Spectral Devices, Inc., USA) ($\lambda = 0.35$–$2.5\,\mu\mathrm{m}$). The details of the measurement procedure were based on the method of Aoki et al. (2000). Use of the obtained spectral albedo in a GSAF (ground-based spectral radiometer system for albedo and flux; Kuchiki et al., 2009) channel with a λ of

1.23 µm allowed us to retrieve the surface optically equivalent snow grain radius (hereafter simply referred to as the "snow grain size" unless otherwise stated) with the GSAF algorithm developed by Kuchiki et al. (2009). In the latest version of this algorithm, the model of snow grain shape can be arbitrarily chosen to be a sphere, spheroid, or Voronoi aggregate. In this study we selected the Voronoi aggregate model developed by Ishimoto et al. (2012), because this choice led to the best agreement with in situ, manually measured surface snow grain size in the case of our data (see Sect. 2.2). We henceforth refer to ~~this~~ these data as snow grain size retrieved by ground-based remote sensing (GRS). We used GRS data for model evaluation (Sect. 4.3).

Figure 2 presents time series of meteorological conditions measured with the AWS during the IOP. Until 9 July, air temperature at 3.0 m above the surface was already high and often exceeded 0 °C in the daytime. The time interval from 10 July until the end of the IOP coincided with the record near-surface melt event period reported by Nghiem et al. (2012); during that time air temperature increased slightly and remained above 0 °C, which is much larger than the estimated possible average air temperature at the SIGMA-A site: −6.5 °C (Sect. 2), continuously (Fig. 2a). The relative humidity with respect to water recorded at 3.0 m above the surface was related to the high air temperature and tended to be high, the values sometimes approaching 100 % (Fig. 2a). At site SIGMA-A, low wind speeds ($< 1.0\,\mathrm{m\,s^{-1}}$) were rarely observed at 3.0 m above the surface during the IOP (Fig. 2b). The gradual day-by-day rise of air temperature was accompanied by a strong southeast wind with a speed sometimes over $10\,\mathrm{m\,s^{-1}}$. Radiation parameters (Fig. 2c) reflect sky conditions. For example, until 3 July and around 9 July, we observed clear-sky conditions on-site. During the clear-sky period, the downward shortwave and near-infrared radiant fluxes showed an obvious diurnal cycle, whereas the downward longwave radiant flux was almost constant. In contrast, cloudy-sky conditions (subjectively observed prevailing cloud types were Cumulus, Stratocumulus, and sometimes Stratus) on 3, 4, 6, 7, and 8 July and after 10 July were characterized by reduced downward shortwave and near-infrared radiant fluxes and increased downward longwave radiant flux. During such conditions, the near-infrared fraction of the downward shortwave radiant flux

decreased to around 0.3, while it was around 0.5 under clear-sky conditions. Neff et al. (2014) examined synoptic-scale atmospheric conditions over the GrIS during July 2012 from various aspects and summarized notable features as follows: (1) warm air originating from a record North American heat wave (the North American drought of 2012 was the worst since 1895), (2) transitions in the Arctic Oscillation, (3) transport of water vapor via an Atmospheric River over the Atlantic to Greenland, and (4) the presence of warm ocean waters south of Greenland. Bonne et al. (2015) clearly showed that moist air mass was advected northward following a narrow band reaching southern Greenland and then it moved northward along the western Greenland coast around 9 July. Observed features of above mentioned meteorological properties during the IOP at the SIGMA-A site are consistent with these large-scale atmospheric conditions.

At the SIGMA-A site, no rainfall was observed on-site until 9 July. After 10 July, we encountered continuous rainfall till 14 July (Aoki et al., 2014b; Yamaguchi et al., 2014). Because precipitation is one of the critical parameters for a snowpack model that is used to calculate mass balance of a snowpack, the total amount of precipitation during 10–14 July was estimated on the basis of precipitation collected with a bucket during the period from 12 July, 20:00 UTC to 14 July, 11:00 UTC, and on the 3 hourly European Centre for Medium-Range Weather Forecasts (ECMWF) Interim reanalysis (ERA-Interim) data (Dee et al., 2011). At first, the precipitation that accumulated in the bucket from 12 July, 20:00 UTC to 14 July, 11:00 UTC and the 3 hourly ERA-Interim reanalysis data were compared. For this comparison, ERA-Interim 1 h accumulated precipitation was simply estimated to be one-third of the 3 hourly accumulated precipitation. The comparison indicated that the accumulated precipitation obtained from the ERA-Interim reanalysis data was lower by a factor of 1/4.9. The most prevailing reason for this discrepancy was not a misrepresentation of the true area of rainfall, but just underestimation by the ERA-Interim reanalysis (Fig. 3). As demonstrated by Chen et al. (2011), ERA-Interim data originally tends to underestimate annual accumulation in the area north of 68°N, even though it shows close spatial pattern of accumulation to the observations over the whole area of GrIS. In addition, it is possible that insufficient horizontal resolution (0.75°) and a hydrostatic atmospheric

model, which cannot reproduce a short-time mesoscale convective system realistically in general, might have caused the large discrepancy. Finally, the precipitation that accumulated between 10 and 14 July, 100 mm, was obtained by multiplying ERA-Interim reanalysis data by a factor of 4.9 (Fig. 2d). According to Ohmura and Reeh (1991), annual total precipitation near the SIGMA-A site is extrapolated to be around 200–300 mm w.e. The estimated total precipitation during this event can account for more than 30–50 % of the annual total precipitation.The procedure to input this information into the SMAP model is described in Sect. 3.3.

2.2 Snow pit measurements

Over the course of the IOP, we performed snow pit observations in the local morning (around 09:30 LT) to be able to characterize the snow physical profiles (Yamaguchi et al., 2014). We also collected near-surface snow samples to measure the mass concentrations of light-absorbing snow impurities such as black carbon (BC) and dust (Aoki et al., 2014b).

The near-surface layer of the snow was recognizable by quite a thick bottom ice layer. We focused on this near-surface layer in the snow pit observations, which were performed every day from 30 June to 13 July, except for 11 and 12 July, when there was heavy rain at the SIGMA-A site. The ~~depth~~ thickness of the layer (above the ice layer) was 88 cm on 30 June. In this paper we refer to this target near-surface layer as the "NSL". At present, the NSL has not been determined to be the latest annual layer, because the lack of justification. Measured properties included profiles of snow grain shape, snow temperature (including bottom ice layer temperature), snow density, volumetric water content, and geometric snow grain size. In addition, the snow grain size of the top 10 cm was measured manually after 1 July. In this snow grain size measurement process, we followed the definition of "r_2" presented by Aoki et al. (2000, 2003, and 2007): one-half the branch width of dendrites or one-half the width of the narrower portion of broken crystals. Figure 4 shows the temporal evolution of the observed snow grain shape profile in the NSL at the SIGMA-A site from 30 June to 13 July 2012. On the whole, until 9 July this layer could be roughly divided into three parts: a bottom layer composed of depth hoar, a middle layer of rounded grains

(sometimes including faceted crystals), and a top layer composed of melt forms, including an ice layer of variable thickness. After 10 July, a wet snow layer expanded from the top to the bottom as the air temperature increased slightly (Fig. 2a), and the rainfall event occurred (Fig. 2d). The measured snow temperature profile is presented in Sect. 4.1 and compared to the results simulated by the SMAP model. In this comparison, total 221 profiles (after rejecting strange data) were available. As for the other snow properties, we used only the data that we obtained on 30 June to specify the initial physical conditions of the snowpack at the SIGMA-A site for the SMAP model simulations. The procedure is briefly explained in Sect. 3.3.

Snow samples to measure the mass concentrations of snow impurities were collected from the top 2 cm and the 2–10 cm layer every other day from 30 June to 12 July (Aoki et al., 2014b). To obtain the mass concentrations of elemental carbon (EC), the samples were melted and filtered on-site, and the filters were weighed and assayed with a carbon analyzer (Lab OC-EC Aerosol Analyzer, Sunset Laboratory Inc., USA). In this study, we assumed, following Aoki et al. (2011), that EC was equivalent to BC. The dust concentrations were determined by subtracting total carbon concentrations from the total impurity concentrations, which were estimated from the difference between the dry weights of the filters before and after filtering (Aoki et al., 2003, 2007). The detailed analytical procedure is precisely described by Kuchiki et al. (2009) and Aoki et al. (2011, 2014b). Figure 5 shows the temporal changes in the mass concentrations of EC and dust in the near-surface snowpack at the SIGMA-A site during the IOP; the EC concentrations increased rapidly after 6 July. Aoki et al. (2014b) have discussed the reasons for this obvious increase, and they concluded that effects of sublimation/evaporation and snow melt amplification due to the low scavenging efficiency of meltwater played an important role.

3 Numerical simulation with the SMAP model

3.1 SMAP model overview

The multilayered physical snowpack model SMAP calculates mass and energy balances of the snowpack by taking snow settlement, phase changes, water percolation, and snow metamorphism into account. The most distinguishing characteristic of the SMAP model is the fact that it incorporates the Physically Based Snow Albedo Model (PBSAM) developed by Aoki et al. (2011). PBSAM calculates snow albedo and the solar heating profile in the snowpack by explicitly considering effects of snow grain size and light-absorbing snow impurities such as BC and mineral dust. In default configuration, the SMAP model requires precipitation ~~,~~ (partitioned in the model into snow and rain by using the algorithm to calculate snow:rain ratios as a function of wet bulb temperature (Yamazaki, 2001)), air pressure, wind speed, air temperature, relative humidity, downward ultraviolet (UV)-visible and near-infrared radiant fluxes, the diffuse components of UV-visible and near-infrared radiant fluxes, downward longwave radiant flux, subsurface heat flux, and the mass concentrations of snow impurities (BC and dust) (Niwano et al., 2012). In the present study, the diffuse components of the UV-visible and near-infrared radiant fluxes were not available, as explained in Sect. 2.1. Under these circumstances, SMAP calculates these fluxes by using the scheme of Goudriaan (1977), together with internally diagnosed cloud fraction calculated from air temperature and simulated net longwave radiant fluxes at the snow surface. The procedure for obtaining cloud fraction is based on the approach of van den Broeke et al. (2004, 2006). Niwano et al. (2014) used data obtained during the winters of 2007–2009 at Sapporo to investigate the effectiveness of the process, and they demonstrated that the accuracy of the simulated snow depth and snow surface temperature were comparable in magnitude to the accuracy of the default configuration.

The main governing equation of the SMAP model is a one-dimensional energy balance equation that takes solar heating of the snowpack and melt-freeze cycles into account (Niwano et al., 2012). This equation is approximated and solved with the Crank–Nicolson finite difference implicit method. In this numerical solution, the SMAP model assumes each model

snow layer to have a thickness d that is allowed to range between d_{min} and d_{max}. The values of d_{min} and d_{max} used in the present study are discussed in Sect. 3.3. Solar heating of the snowpack was calculated with a component of PBSAM. Input requirements for this component include internally calculated profiles of snow grain size and snow water equivalent (SWE), as well as the mass concentrations of snow impurities given externally from in situ measurements or host global or regional circulation models. Snow grain size was calculated by employing a model geometry that envisions two spherical ice particles connected by a neck (Lehning et al., 2002). By calculating the specific surface area (SSA) of snow per unit volume with the nonspherical model geometry, SMAP obtains snow grain size. Temporal evolution of snow grain size is governed by following three types of metamorphism regimes: equi-temperature metamorphism, temperature-gradient metamorphism, and wet snow metamorphism. The formulation of these metamorphism laws is based on results from the SNOWPACK model (Lehning et al., 2002). Furthermore, the SMAP model implicitly takes into account the effects of snow metamorphism under alternating temperature gradients (small rounded grains can be formed even when the temperature gradient is large if the sign of the temperature gradient changes with a 24-h cycle.) (Pinzer and Schneebeli, 2009) by forcing temperature gradient metamorphism, which generally induces rapid grain growth, not to occur in the top 20 cm of the each model layer.

Recently, the SMAP model was updated with respect to water movement in the snowpack, snow settlement, and turbulent heat exchanges under very stable conditions (Niwano et al., 2014). Water movement in the snowpack is now governed by the Richards equation (Richards, 1931), which takes into consideration Darcy's law; hydraulic diffusivity and hydraulic conductivity are calculated by the van Genuchten model (van Genuchten, 1980) adapted to snow (Shimizu, 1970; Hirashima et al., 2010; Yamaguchi et al., 2010, 2012). As for snow settlement, the updated version of the SMAP model calculates the viscosity coefficient of snow using the scheme presented by Vionnet et al. (2012), which was developed to improve the performance of the Crocus model (Brun et al., 1989, 1992; Vionnet et al., 2012; Carmagnola et al., 2014). To ensure ~~minimum~~ small but non-zero turbulent heat exchanges under very stable conditions, we set an upper bound of 0.1 on the Richardson number.

During IOP, low wind speed were rarely observed at the SIGMA-A site as mentioned in Sect. 2.1. As a result, preliminary numerical simulation revealed that the impact of the upper bound was not clear during IOP; however, it is still set in this study.

3.2 Adaption of the SMAP model to the Greenland snowpack

In this section we discuss the adaptation of the model that enabled the SMAP model to be suitable for polar (especially Greenland) snowpack simulations. To simulate the temporal evolution of snow temperature accurately by solving the one-dimensional energy balance equation in the snowpack, the thermal conductivity of snow k_{eff} (W m^{-1} k^{-1}) should be assigned an appropriate value. In this study, we employed the parameterization of Anderson (1976) that describes k_{eff} as a function of snow density ρ_{s} (kg m^{-3}):

$$k_{\mathrm{eff}} = 0.021 + 2.5 \left(\frac{\rho_{\mathrm{s}}}{1000} \right)^2, \tag{1}$$

an equation that is widely used in polar regions (e.g., van den Broeke et al., 2005; Kuipers Munneke et al., 2009; van As, 2011; Brun et al., 2011).

The snow surface roughness length ~~of~~ for momentum z_0 affects turbulent heat exchanges between the snow surface and the atmosphere. Brock et al. (2006) compiled published data of z_0 and demonstrated that the values were quite dependent on surface conditions and places. Considering this, we assumed following constant values for z_0 (mm):

$$z_0 = \begin{cases} 0.12 & \text{for snow before melting} \\ 1.3 & \text{for snow after melting} \end{cases}, \tag{2}$$

which was presented by Greuell and Konzelmann (1994) and they simulated the mass balance and englacial temperature at the ETH Camp, west Greenland, during the 1990 summer melting period with these values. During IOP, the surface condition at SIGMA-A was smooth. van den Broeke et al. (2009) presented time series of z_0 at sites S5 (490 m a.s.l.), S6 (1020 m a.s.l.), and S9 (1520 m a.s.l.) on the K-transect in southwest Greenland during

August 2003 to August 2007. The above mentioned values for z_0 (Eq. 2) fall in the range of their result at S9, where surface condition was relatively smooth. The uncertainty of the SMAP model calculated SEB caused by the choice of z_0 is investigated in Sect. 5. In the SMAP model, roughness lengths for heat and moisture are calculated following Andreas (1987) as explained by Niwano et al. (2012).

3.3 Model configuration

In the present study we calculated the temporal evolution of snow physical states in the NSL (see Sect. 2.2) at the SIGMA-A site from 30 June 2012, 16:45 UTC to 14 July 2012, 12:00 UTC. To perform detailed model simulations we divided the NSL into several thin model layers. According to Dadic et al. (2008), the recommended model vertical resolution for an Arctic snowpack is on the order of 10 mm, because there is a strong feedback between small-scale snow structure and snow temperature that should be simulated accurately by snowpack models. Based on this consideration, the SMAP model vertical layer thickness (see Sect. 3.1) used in this study ranged between $d_{\mathrm{min}} = 2$ mm and $d_{\mathrm{max}} = 6$ mm. Accordingly, it became necessary for the time step of the numerical integration Δt to be shortened. Thus, Δt was set to 30 s in the present study.

Input parameters used to drive the SMAP model in the present study were air pressure; air temperature and relative humidity at 3.0 m above the snow surface (Fig. 2a); wind speed at 3.0 m above the snow surface (Fig. 2b); downward shortwave, near-infrared, and longwave radiant fluxes (Fig. 2c); accumulated precipitation (Fig. 2d); the temperature of the thick bottom ice layer in the NSL (lower boundary condition); and the mass concentrations of snow impurities (Fig. 5). In addition, the emissivity of the snow surface ε_{s} was assumed to be 0.98 (Armstrong and Brun, 2008; van As, 2011) throughout this study.

The time interval for meteorological properties was selected to be 5 min, whereas daily values were used for other properties. The corrected three-hourly accumulated precipitation data were divided equally into each time interval. Regarding the measured mass concentrations of snow impurities (Fig. 5), we followed the same method used by Niwano et al. (2012), who equated the values in the top 2 cm of the model layers of the snowpack to the corre-

sponding observed values and assigned the observed values in the 2–10 cm depth interval equally to the lower model layers. During the period when measurements of the mass concentrations of snow impurities were unavailable (dashed lines in Fig. 5), we used the values measured at the nearest point in time. The initial physical states of the snowpack in the NSL on 30 June (profiles of snow grain shape, snow temperature, snow density, volumetric water content, and geometric snow grain size) were taken from the snow pit observations conducted on 30 June 2012, 16:45 UTC (Yamaguchi et al., 2014). These observations were distributed within the model layers, and the layer thickness d was in all cases set to 5 mm in the NSL at that time. Because the SMAP model calculates shortwave albedo as a function of snow grain size and the mass concentrations of snow impurities, information regarding an optically equivalent snow grain size profile was necessary. In the present study, an optically equivalent profile was obtained by multiplying the geometric profile by a factor that produced agreement between the calculated shortwave albedo and observations on 30 June 2012, 16:45 UTC. The assigned factor was 0.88.

4 Model evaluation using the data at the SIGMA-A site

In this section we evaluate the SMAP model using the data measured at the SIGMA-A site during the IOP to adapt it to the GrIS snowpack. The following parameters were validated quantitatively: snow temperature profile, snow surface temperature, surface snow grain size, and shortwave albedo. When a measured snow temperature profile was compared against simulation results, the depth of the NSL simulated by the model (the SMAP model tended to underestimate the NSL's depth by -2.0 cm compared to the snow pit measurements during the IOP) was adjusted to the measured depth as a post-process, where model simulated internal properties were not modified at all. The measured snow surface temperature T_{s0} was calculated from the following relationship between the observed downward and upward longwave radiant fluxes ($L^{\downarrow}$ and $L^{\uparrow}$):

$$L^{\uparrow} = \varepsilon_s \sigma T_{s0}^4 + (1 - \varepsilon_s) L^{\downarrow}, \quad (3)$$

where ~~ε_s is the emissivity of the snow surface, and~~ σ is the Stefan–Boltzmann constant. ~~In the present study, we assumed $\varepsilon_s = 0.98$ (Armstrong and Brun, 2008).~~ The model performance was assessed in terms of the root mean square error (RMSE) and mean error (ME) (Table 1). In this paper ME is defined as the average difference between simulated and observed values.

4.1 Snow temperature profile

We first examined whether the SMAP model could reproduce the internal physical states of the NSL in terms of the snow temperature profile. Model performance during the IOP (Table 1) indicated that the model ~~tended to underestimate the snow temperature profile. However, the SMAP model satisfactorily~~ simulated the temperatures reasonably. An example profile comparison on 8 July showed that the top 40 cm of the observed snowpack was wet (Fig. 6), and the condition was reproduced by the SMAP model. Even when such observed wet snow conditions were excluded from the statistical assessment of model performance, the order of magnitude of the RMSE and ME did not change (Table 1).

4.2 Snow surface temperature

Snow surface temperature affects all energy flux components of the SEB, except for the net shortwave radiant flux. A comparison of observed and simulated snow surface temperatures during the IOP (Fig. 7) as well as the obtained MEs (Table 1) indicated that the SMAP model tended to overestimate snow surface temperature; however, the RMSE obtained in this study (~~0.53~~0.58 °C) was an improvement compared to the previous study by Niwano et al. (2012) at Sapporo during the winters of 2007–2009 (2.45 and 2.3 °C for the winters of 2007–2008 and 2008–2009, respectively). In this case as well, scores under dry snow surface conditions were still reasonable (RMSE ~~= 0.85~~ = 0.94 °C, and ME ~~= 0.55~~ = 0.68 °C). These foregoing statistics are almost the same order of magnitude as the analogous statistics from previous, detailed snow modeling studies performed in polar regions (Kuipers Munneke et al., 2009, 2012; Brun et al., 2011).

4.3 Surface snow grain size

For the SMAP model, snow grain size is one of the key parameters to be simulated accurately, because the SMAP model calculates the snow albedo and solar heating profile in the snowpack using the PBSAM, to which snow grain size is an input parameter. Figure 8a depicts the simulated snow grain size profile in the NSL, and Fig. 8b compares the surface snow grain size determined from in situ manual measurements and GRS against the simulation result. Because the GRS estimates agreed well with in situ measurements, and because we could obtain more data from GRS than from in situ manual measurements, model validation was performed against GRS data in the present study. The simulated surface snow grain size sometimes decreased abruptly (Fig. 8b), although a new snowfall event was not observed during the IOP. The abrupt decrease in grain size was caused by rapid surface melting and subsequent continuous exposure of layers beneath that were simulated by the SMAP model (Fig. 8a). The order of magnitude of the simulated snow grain size was almost the same with the SMAP model and GRS, and the RMSE (0.21 mm) and ME (~~0.16~~0.17 mm) (Table 1) were almost the same order of magnitude as the analogous errors reported by Niwano et al. (2012) for seasonal snow simulations at Sapporo, Japan, during the winters of 2007–2009 (RMSE $= 0.31$ and 0.15 mm, and ME $= -0.04$ and -0.02 mm, for the winters of 2007–2008 and 2008–2009, respectively). During 3–5 July, when we observed surface hoar with small grains of snow on the surface at the SIGMA-A site (Yamaguchi et al., 2014), discrepancies between observations and simulations stood out (Fig. 8b). The reason for this failure is that the SMAP model could not simulate surface hoar formation during this period. In the SMAP model surface hoar is created when the latent heat flux is positive and the wind speed is less than $3\,\mathrm{m\,s^{-1}}$ (Föhn, 2001); however, the simulated H_L from the night of 2 July to the morning of 5 July was continuously negative (more detailed discussion follows in Sect. ~~5~~6.2).

In the SMAP model, the latent heat flux is calculated on the assumption that the snow surface is saturated (Niwano et al., 2012), an assumption that is widely made by many physical snowpack models. However, as Box and Steffen (2001) have pointed out, this

method can detect surface hoar deposition only in cases of extreme temperature inversion, and this limitation leads to underestimation of surface hoar. Because this result suggests that reconsideration of the method of calculating the latent heat flux in the SMAP model is necessary to obtain an accurate SEB, we discuss this topic further in Sect. ~~5.~~ 6.2.

4.4 Shortwave albedo

Now we focus on the shortwave albedo, which is another important parameter for estimating snow-atmosphere interactions as well as snow surface temperature. Figure 9 compares observed shortwave albedos with albedos simulated with the SMAP model during the IOP. The comparison shows that the SMAP model successfully reproduced the observed diurnal variations. The RMSE and ME in Table 1 support this assessment. Furthermore, the SMAP model simulated observed spikes when snow albedo rapidly increased, especially around 4 July and after 10 July. The cause of these spikes is the fact that the snow albedo is generally higher under cloudy-sky than under clear-sky conditions (Liljequist, 1956; Yamanouchi, 1983; Aoki et al., 1999). These results imply that the component of the PBSAM driven by the observed near-infrared and UV-visible fractions of the downward shortwave radiant flux, as well as the diffuse fractions calculated by the procedure described in Sect. 3.1, played an important role in improving the precision of the SMAP model simulations. Therefore, once the SMAP model or the PBSAM are coupled with atmospheric models, it is necessary for such host atmospheric models to simulate the presence or absence of cloud realistically. King et al. (2014) also argued that efforts to improve model simulations of surface energy balance and melt in the polar region should concentrate initially on reducing biases in modeled shortwave and longwave radiation, which are caused by deficiencies in the representation of cloud properties.

In Sect. 4.3, however, we found clear discrepancies between observed and simulated surface snow grain size, especially during 3–5 July, when simulated shortwave albedo agreed well with observations. This paradox can be explained as follows: as demonstrated by Yamanouchi (1983), the difference between the downward near-infrared radiant fluxes under clear-sky and cloudy-sky conditions is larger than the analogous difference in the down-

ward visible radiant fluxes. The explanation is that most of the absorption of solar radiation by clouds occurs in the near-infrared region, and the difference in multiple reflection effects due to the spectral differences of surface albedo magnifies the impact of this preferential near-infrared absorption. Figure 2c depicts the observed near-infrared fraction of the downward shortwave radiant flux. Actually, the near-infrared fraction was depleted during the cloudy-sky conditions observed on 3, 4, 6, 7, and 8 July and after 10 July (Sect. 2.1). In the PBSAM, the shortwave albedo is calculated from a weighted summation of visible albedo and near-infrared albedo. The weights for these albedos are the visible and near-infrared fractions of the downward shortwave radiant flux (Aoki et al., 2011). A decrease of the near-infrared fraction therefore increases the influence of the visible albedo on the calculated shortwave albedo, and the influence of the near-infrared albedo, which is mainly affected by snow grain size (Wiscombe and Warren, 1980), decreases. The simulated shortwave albedo therefore agreed with observations, even during 3–5 July, when the SMAP model could not reproduce surface hoar and the associated small near-surface snow grain size.

5 Reconsideration of the latent het flux calculation method

As discussed in Sect. 4.3, calculation of the latent heat flux H_L based on the assumption of the SMAP model that the snow surface is saturated might lead to underestimation of surface hoar deposition. Here we refer to this method as 1LM, in accordance with Box and Steffen (2001). According to Box and Steffen (2001), employing two-level atmospheric data to calculate H_L can solve this problem, an approach we designate as the 2LM method. As noted in Sect. 2.1, the SIGMA-A AWS measured temperature, relative humidity, and wind speed at heights of 3 and 6above the surface. In this section we calculate the latent heat flux using the AWS data at these two heights, and we investigate whether the SMAP model can simulate surface hoar formation with small snow grain sizes by using the 2LM method.

The original formulation of H_{L} employed by the SMAP model (1LM) is based on the bulk method and is expressed as follows (Niwano et al., 2012):

$$H_{\mathsf{L}} = \frac{\rho_{\mathsf{a}} L_v \kappa^2 u_1 \left(q_1 - q_{\mathsf{s}0}\right)}{\left[\ln\left(\frac{z_1}{z_0}\right) - \Psi_{\mathsf{M}}\left(\frac{z_1}{L}\right)\right]\left[\ln\left(\frac{z_1}{z_Q}\right) - \Psi_{\mathsf{H}}\left(\frac{z_1}{L}\right)\right]},$$

where ρ_{a} is the density of air, L_v is the latent heat of sublimation or evaporation, κ is the von Krmn constant, u_1 is the wind speed at a measurement height z_1 (in this study, z_1 is 3), q_1 and $q_{\mathsf{s}0}$ are the specific humidity at z_1 and the snow surface, respectively, Ψ_{M} and Ψ_{H} are profile functions for momentum and heat, respectively, z_0, and z_Q are roughness lengths for momentum and moisture, respectively, and L is the Obukhov length. If we now use atmospheric data at two heights (z_1 and z_2; z_2 is 6in this study), the formulation of the bulk method with the 2LM model can be rewritten as follows:

$$H_{\mathsf{L}} = \frac{\rho_{\mathsf{a}} L_v \kappa^2 \left(u_2 - u_1\right)\left(q_2 - q_1\right)}{\left[\ln\left(\frac{z_2}{z_1}\right) - \Psi_{\mathsf{M}}\left(\frac{z_2}{L}\right) + \Psi_{\mathsf{M}}\left(\frac{z_1}{L}\right)\right]\left[\ln\left(\frac{z_2}{z_1}\right) - \Psi_{\mathsf{H}}\left(\frac{z_2}{L}\right) + \Psi_{\mathsf{H}}\left(\frac{z_1}{L}\right)\right]},$$

where u_2 and q_2 are the wind speed and specific humidity at z_2, respectively. The three unknown parameters L, Ψ_{M}, and Ψ_{H} can be calculated by the same method used by Niwano et al. (2012).

Figure 10a shows the temporal changes of the 1h averaged latent heat fluxes calculated from two-level atmospheric measurements using the 2LM (OBS) compared to the original SMAP simulation result (SMAP). The former obviously tends to be higher than the latter, and sometimes the signs of the fluxes are different. Because the SMAPuses the simulated snow surface temperature to obtain the latent heat flux, the above mentioned discrepancy can be attributed to error of simulated snow surface temperature. We therefore also investigated the latent heat flux calculated from the atmospheric data measured at only one height (3) above the surface as well as the observed snow surface temperature obtained with Eq. (3) (OBSin Fig. 10a). The result indicated that the latent heat flux from SMAPwas almost compatible

with the heat flux OBS, and the discrepancy depended mainly on the choice of the 1LM or 2LM method. This dependency is also apparent in the results of Box and Steffen (2001).

As mentioned in Sect. 3.2, we assumed constant values for z_0 (0.12 and 1.3for snow before and after melting, respectively) following Greuell and Konzelmann (1994) in this study. However, as Braithwaite (1995) pointed out, the uncertainty in z_0 causes significant error in turbulent heat flux calculations. Therefore, in order to confirm results from 1LM and 2LM are significantly different, we performed numerical sensitivity tests based on OBS, where value of z_0 was perturbed between the possible maximum and minimum values. These values were determined as follows: from the compilation by Brock et al. (2006), the maximum value for z_0 of the GrIS snow surface was found to be around 10, while we assumed the minimum value for z_0 of the GrIS snow surface to be around 0.01based on the results by Smeets and van den Broeke (2008). Figure 10b compares latent heat flux from OBSusing the default configuration of z_0 with those from above mentioned two sensitivity tests with z_0 values of 10 and 0.01. In general, absolute value of the latent heat flux was increased with the condition that z_0 was set to be 10(mean difference against the original OBSwas −1.4), while it was reduced if z_0 was set to be 0.01(mean difference against the original OBSwas 3.8). However, it is still obvious that characteristics of latent heat fluxes with perturbed z_0 are significantly different from the results from OBS.

We next performed another numerical simulation with the SMAP model (SMAP). In this case the latent heat flux, which was used to assess surface hoar formation and to provide a boundary condition for the governing one-dimensional diffusion equation in the SMAP model (Niwano et al., 2012), was determined directly from the OBScase. Figure 10c compares the surface snow grain size from the SMAPcase with the surface snow grain size from the SMAPcase and GRS. A difference between results of the SMAPand SMAPcases is apparent on 4 July (Fig. 10c), when snow grain size is lower for the SMAPcase than for the SMAPcase. The low grain size estimated with SMAP(< 0.4) can be attributed to modeled surface hoar formation. Actually, the latent heat flux simulated with OBSon 4 July was positive (Fig. 10a), and the winds at 3above the surface around 4 July were calm (Fig. 2b). These conditions are suitable for modeled surface hoar formation, as explained in

Sect. 4.3. We also investigated the accuracy with which SMAPsimulated the snow surface temperature and shortwave albedo, which control the SEB. The RMSE for the snow surface temperature was 0.54C, and the shortwave albedo was 0.026. These results are almost equivalent to the results from SMAP(Table 1) and demonstrate that input of two-level atmospheric measurements into a physical snowpack model is much preferable to driving the model with one-level atmospheric measurements; the former method is much more likely to detect surface hoar.

Although SMAPsucceeded in reproducing the surface hoar detected at the SIGMA-A site during the IOP, there were still obvious discrepancies with GRS results around 2–5 July (Fig. 10c). To resolve this problem, it might be necessary to consider the possibility of a new snow grain size for surface hoar, which is now calculated as a function of air temperature in the same manner as new snowfall (Niwano et al., 2012).

5 SEB during the IOP at SIGMA-A

FinallyNow, we look into the SEB during the IOP at the SIGMA-A site to elucidate the physical conditions of both the snowpack and the atmosphere that led to the remarkable melting around 12 July, when the record near-surface melt occurred over more than 95 % of the entire surface of the GrIS (Nghiem et al., 2012). The SEB equation (Armstrong and Brun, 2008) can be written as follows:

$$S_{\mathrm{net}} + L_{\mathrm{net}} + H_{\mathrm{S}} + H_{\mathrm{L}} + H_{\mathrm{R}} + H_{\mathrm{G}} = Q_{\mathrm{net}}, \tag{4}$$

where S_{net} is the net shortwave radiant flux, L_{net} is the net longwave radiant flux, H_{S} is the sensible heat flux, H_{L} is the latent heat flux, H_{R} is the heat flux associated with rainfall , calculated as a function of rainfall rate and a difference in rain temperature (wet bulb temperature is assumed) and surface temperature (Niwano et al., 2012), H_{G} is the subsurface conductive heat flux and Q_{net} is the net energy flux at the snow surface. As already mentioned, these fluxes are defined to be positive when they are directed into the snow surface. The snow surface is heated when the flux is positive and surface melt is occurred

if the surface temperature is 0 °C, whereas it is cooled if the flux is negative. In this study, S_{net} and L_{net} were calculated from in situ measurements. Other fluxes on the left-hand side of Eq. (6) were estimated as a function of measured snow surface temperature by using the SMAP model. ~~However, based on the discussion in Sect. 5, only H_L was calculated by using the 2LM approach.~~

~~Figure 11~~ Figure 10 shows the temporal changes of the 1 h averaged simulated SEB during the IOP. S_{net} remained positive throughout the IOP. L_{net} was negative for much of the time prior to 9 July but was positive most of the time after 10 July. H_S was close to 0 W m^{-2} until 9 July, but it gradually increased after 10 July and sometimes reached about 50 W m^{-2}. The other turbulent heat flux, H_L, was negative most of the time during the first half of the IOP, but it ~~increased~~ became generally positive after 10 July as well. After 10 July there was heavy rainfall frequently, but its impact on the SEB was quite small (H_R was less than 10 W m^{-2} most of the time, although it sometimes reached more than 15 W m^{-2}). Finally, H_G showed clear diurnal variation: it heated the surface especially during the night time, while it was almost 0 W m^{-2} in the daytime as a result of isothermal profile in the near-surface snowpack caused by meltwater percolation. As a result, until 9 July the total surface energy flux, Q_{net}, clearly varied diurnally, being negative during the night and positive during the day. However, after 10 July it remained positive at all times.

Because there was a clear contrast in the calculated SEB characteristics during the period from 30 June to 9 July ("Period-1") and the time interval 10–14 July ("Period-2"), we compared the average SEB components between Period-1 and Period-2 (Fig. ~~12~~11) to characterize the SEB at the SIGMA-A site around 12 July, when continuous melting was observed. Figure ~~12~~ 11 reveals dramatic modulations of both S_{net} and L_{net}, and changes in H_S and H_L were also remarkable. Quantitatively, there were significant positive increments in H_S (4.0 to ~~15.2~~15.3 W m^{-2}; +11.3 W m^{-2}), H_L (~~−13.2 to 17.8~~18.0 to 7.2 W m^{-2}; ~~+31.0~~25.2 W m^{-2}), and L_{net} (−54.9 to 2.1 W m^{-2}; +57.1 W m^{-2}), the total positive increment being ~~102.5~~96.7 W m^{-2}. There was a remarkable decrease only in S_{net} (83.0 to 40.7 W m^{-2}; −42.3 W m^{-2}). As a result, Q_{net} increased by ~~55.0~~49.1 W m^{-2} (~~24.9 to 79.9~~20.1 to 69.2 W m^{-2}). These values, calculated during Period-1, are almost equal to the

surface fluxes from June to August averaged during the summers of 2000–2011 over the GrIS accumulation area based on the MAR regional climate model (Fettweis et al., 2011) and MODIS data presented by Box et al. (2012). On the other hand, the SEB characteristics during Period-2 (signs and orders) resemble those obtained at Langfjordjøkelen, Norway (Giesen et al., 2014).

The decrease of S_{net} was due to both a reduction of downward shortwave radiant flux (352.7 to 203.9 W m^{-2}) and a slight increase in shortwave albedo from 0.775 to 0.810. The latter value is as high as the 2000–2011 summer (June to August) average albedo over the GrIS accumulation area (0.809) reported by Box et al. (2012) and the cause of increase was due mainly to the appearance of clouds (discussed in Sect. 4.4). Modulation of H_{S} was caused mainly by an increase of temperature, which is clearly apparent in Fig. 2a. The cause of the increase in H_{L} was basically the same: increases in relative humidity and air temperature. The latter reached more than 0 °C. The abrupt transition of radiative properties is understandable from the perspective of cloud radiative forcing (defined as the difference in net surface radiant fluxes under cloudy-sky and clear-sky conditions) in the polar region: at the snow surface shortwave cloud radiative forcing is negative, and longwave cloud radiative forcing is positive (Aoki and Yamanouchi, 1992). We thus conclude that the appearance of low-level clouds (Sect. 2.1) accompanied by a remarkable increase of temperature (Fig. 2a) played an important role and induced surface heating during Period-2. The heating occurred via a large increase in L_{net}, which was able to substantially compensate for the reduction of S_{net}. Bennartz et al. (2013) have investigated the effect of clouds on the temporal development of surface temperature by performing numerical sensitivity tests with a prognostic surface energy balance model and by parameterizing downward radiant fluxes at the surface. They have argued that low-level, liquid clouds played a critical role in the enhancement of surface melting at Summit, Greenland by increasing near-surface temperature through their radiative effects. The present results, which highlight the importance of low-level clouds, are consistent with their conclusion.

6 Discussion

In this section, we investigate uncertainties in the calculated SEB that can be induced by model settings and calculation methods of the SMAP model. The purpose of this work is to confirm the validity of SEB characteristics presented in Sect. 5. Because S_{net} and L_{net} are directly given from in-situ measurements (mentioned in Sect. 5), uncertainties only related to turbulent heat fluxes are discussed here.

6.1 Effects of model settings on the calculated SEB

As mentioned in Sect. 3.2, we assumed constant values for z_0 (0.12 and 1.3 mm for snow before and after melting, respectively) following Greuell and Konzelmann (1994) in this study. However, as Braithwaite (1995) pointed out, the uncertainty in z_0 causes significant error in turbulent heat flux calculations. Therefore, we performed numerical sensitivity tests based on the SEB calculation performed in Sect. 5, where value of z_0 was perturbed between the possible maximum and minimum values. These values were determined as follows: from the compilation by Brock et al. (2006), the maximum value for z_0 of the GrIS snow surface was found to be around 10 mm, while we assumed the minimum value for z_0 of the GrIS snow surface to be around 0.01 mm based on the results by Smeets and van den Broeke (2008). Compared to the original run (H_{S} and H_{L} during IOP were estimated to be 7.6 W m^{-2} and -10.0 W m^{-2}, respectively), results from sensitivity studies revealed that absolute values of the turbulent heat fluxes were increased with the condition that z_0 was set to be 10 mm (mean differences against the original SEB calculation were 0.8 W m^{-2} and -1.4 W m^{-2} for H_{S} and H_{L}, respectively; the same tendency was also reported by van As (2011)), while they were reduced if z_0 was set to be 0.01 mm (mean differences against the original SEB calculation were -2.9 W m^{-2} and 3.8 W m^{-2} for H_{S} and H_{L}, respectively). However, these uncertainties still do not affect characteristics of temporal changes in SEB during IOP at the SIGMA-A site discussed in Sect. 5 so much.

Secondly, we investigated effects of ε_{s} introduced in Sect. 3.3 on SEB calculations. In this sensitivity test, ε_{s} was set to be 1.0 and surface temperature (to be input to the SMAP

model) was calculated only from observed $L^{\uparrow}$. The result indicated that mean differences of turbulent heat fluxes against the original SEB calculation were 1.1 W m^{-2} and 0.9 W m^{-2} for H_S and H_L, respectively. This result implies that the sensitivity of SEB calculation to the choice of ε_s is small, and SEB characteristics during IOP at the SIGMA-A site presented in Sect. 5 is still valid. van As (2011) also performed this type of sensitivity test and demonstrated ε_s's small impact on the SEB calculation.

6.2 Uncertainties caused by the latent het flux calculation method

As discussed in Sect. 4.3, calculation of the latent heat flux H_L based on the assumption that air at the surface is saturated with respect to ice at the snow surface temperature might lead to underestimation of surface hoar deposition, which implies that internally diagnosed H_L in the SMAP model simulation presented in Sect. 4 can be underestimated. Here we refer to this method as 1LM, in accordance with Box and Steffen (2001). According to Box and Steffen (2001), employing two-level atmospheric data to calculate H_L can solve this problem, an approach we designate as the 2LM method. As noted in Sect. 2.1, the SIGMA-A AWS measured temperature, relative humidity, and wind speed at heights of 3 and 6 m above the surface. In this section we calculate the latent heat flux using the AWS data at these two heights, and we investigate whether the SMAP model can simulate surface hoar formation with small snow grain sizes by using the 2LM method.

The original formulation of H_L employed by the SMAP model (1LM) is based on the bulk method and is expressed as follows (Niwano et al., 2012):

$$H_L = \frac{\rho_a L_v \kappa^2 u_1 (q_1 - q_{s0})}{\left[\ln\left(\frac{z_1}{z_0}\right) - \Psi_M\left(\frac{z_1}{L}\right)\right]\left[\ln\left(\frac{z_1}{z_Q}\right) - \Psi_H\left(\frac{z_1}{L}\right)\right]}, \quad (5)$$

where ρ_a is the density of air, L_v is the latent heat of sublimation or evaporation, κ is the von Kármán constant, u_1 is the wind speed at a measurement height z_1 (in this study, z_1 is 3 m), q_1 and q_{s0} are the specific humidity at z_1 and the snow surface, respectively, Ψ_M and

Ψ_H are profile functions for momentum and heat, respectively, z_0, and z_Q are roughness lengths for momentum and moisture, respectively, and L is the Obukhov length. If we now use atmospheric data at two heights (z_1 and z_2; z_2 is 6 m in this study), the formulation of the bulk method with the 2LM model can be rewritten as follows:

$$H_L = \frac{\rho_a L_v \kappa^2 (u_2 - u_1)(q_2 - q_1)}{\left[\ln\left(\frac{z_2}{z_1}\right) - \Psi_M\left(\frac{z_2}{L}\right) + \Psi_M\left(\frac{z_1}{L}\right)\right]\left[\ln\left(\frac{z_2}{z_1}\right) - \Psi_H\left(\frac{z_2}{L}\right) + \Psi_H\left(\frac{z_1}{L}\right)\right]}, \quad (6)$$

where u_2 and q_2 are the wind speed and specific humidity at z_2, respectively. Other parameters are calculated by the same method used by Niwano et al. (2012). The choice of Ψ_M and Ψ_H depends on stability conditions in the atmospheric boundary layer. When the atmosphere is stable, the SMAP model assumes that $\Psi_M = \Psi_H$ and calculates the profile functions according to Holtslag and De Bruin (1988), whereas the SMAP model carries out the calculations with functions determined by Paulson (1970) under unstable conditions.

Figure 12a shows the temporal changes of the 1 h averaged latent heat fluxes calculated from two-level atmospheric measurements using the 2LM (OBS_2LM) compared to the result presented in Sect. 5 (OBS_1LM) as well as original SMAP simulation result (SMAP_1LM) presented in Sect. 4. Obviously, the result indicated that the latent heat flux from OBS_1LM was almost compatible with the heat flux from SMAP_1LM, implying that the OBS_1LM is also likely to underestimate the latent heat flux. Comparison between OBS_2LM and OBS_1LM shows that the former obviously tends to be higher than the latter, and sometimes the signs of the fluxes are different. According to previous studies (Box and Steffen, 2001; Cullen et al., 2014), the sign and magnitude of the latent heat fluxes from the 1LM and 2LM methods agree reasonably at low elevations on the GrIS, whereas they often differ from each other at the higher elevations. Measurements conducted previously in the northwest GrIS (the Humboldt and GITS sites) showed that the net annual sublimation from the 1LM and 2LM methods did not agree sufficiently at both sites (Box and Steffen, 2001). In the former site, the sign was contrasting, while the magnitude was remarkably different at the latter site.

We next performed another numerical simulation with the SMAP model (SMAP_2LM), where shortwave albedo and snow surface temperature were simulated with the same manner as performed in Sect. 4. In this case, the latent heat flux determined directly from the 2LM method was used only for the assessment of surface hoar formation, while that from the 1LM method was employed for a boundary condition of the governing one-dimensional diffusion equation in the SMAP model (Niwano et al., 2012). Figure 12b compares the surface snow grain size from the SMAP_2LM case with the surface snow grain size from the SMAP_1LM case and GRS. A difference between results of the SMAP_2LM and SMAP_1LM cases is apparent on 4 July (Fig. 12b), when snow grain size is lower for the SMAP_2LM case than for the SMAP_1LM case. The low grain size estimated with SMAP_2LM (< 0.4 mm) can be attributed to modeled surface hoar formation. Actually, the latent heat flux simulated with OBS_2LM on 4 July was positive (Fig. 12a), and the winds at 3 m above the surface around 4 July were calm (Fig. 2b). These conditions are suitable for modeled surface hoar formation, as explained in Sect. 4.3. Although SMAP_2LM succeeded in reproducing the surface hoar detected at the SIGMA-A site during the IOP, which implies that the 2LM method calculated latent heat flux might be more probable than that from the 1LM method, there were still obvious discrepancies with GRS results around 2–5 July (Fig. 12b). To resolve this problem, it might be necessary to consider the possibility of a new snow grain size for surface hoar, which is now calculated as a function of air temperature in the same manner as new snowfall (Niwano et al., 2012).

According to Box and Steffen (2001), the uncertainty of the 2LM method increases as the temperature, humidity, and wind speed differences between two measurement heights decrease. These motivated us to investigate the significance of the 2LM method calculated latent heat flux during IOP. In this inquiry, gradients (positive downward) of wind speed, temperature, and vapor pressure between the surface and the lower measurement height, as well as those between the lower and upper measurement heights were investigated at first. Averaged gradients between the surface and the lower measurement height during the IOP were $1.6\,\mathrm{s}^{-1}$, $0.3\,^{\circ}\mathrm{C\,m}^{-1}$, and $-0.15\,\mathrm{hPa\,m}^{-1}$, respectively. The value for vapor pressure is very close to that obtained at Summit during 2000–2002 reported by Cullen et al.

(2014). On the other hand, averaged gradients between the lower and upper measurement heights were nearly 0, except for the case of wind speed: $0.2\,s^{-1}$. Focusing on the period from 00:10 to 00:20 UTC on 4 July when SMAP_2LM detected the surface hoar, vapor pressure gradients showed opposite signs: $-0.13\,hPa\,m^{-1}$ for the 1LM method and $0.01\,hPa\,m^{-1}$ for the 2LM method, respectively. Although this result explains the reason why only the 2LM method succeeded in the surface hoar detection, the latter value is still very small. These make it difficult to assess uncertainties of the 2LM method caused by each sensor as expected. In fact, numerical sensitivity studies with perturbed input parameters considering absolute accuracy of temperature, relative humidity, and wind speed sensors ($\pm 0.2\,°C$, $\pm 2\,\%$, and $\pm 0.3\,m\,s^{-1}$, respectively) in the 2LM calculation modified the picture of calculated turbulent heat fluxes drastically in any calculations. Even when relative differences in the accuracy of two sensors at the lower and upper measurement heights were considered (according to our relative calibration of the instruments performed in advance, air temperature and wind speed sensors at two levels showed no significant difference; however, as for relative humidity, the upper sensor tended to be lower by 1.2 % compared to the lower sensor), differences in calculated latent heat flux with perturbed input parameters were quite large as well. Therefore, we should conclude that underestimation of the latent heat flux calculated with the 1LM method could be plausible, although the exact order of underestimation was quite hard to detect during this study period.

7 Conclusions

In this study, we investigated the record near-surface melt event that occurred over the GrIS during the IOP (30 June to 14 July 2012) from the standpoint of the SEB. We used data measured in situ at the SIGMA-A site, where significant increases of air temperature, relative humidity, and downward longwave radiant flux, as well as heavy rainfall and abrupt near-surface snowmelt, were observed beginning on 10 July. Although radiation-related components of the SEB could be determined from AWS data, other fluxes were not measured directly. We therefore employed the physical snowpack model SMAP to calculate the

H_S, H_L, and H_R. Because this was the first attempt to adapt the SMAP model to a polar region, we carried out a preliminary analysis of various aspects of the performance of the SMAP model. We calculated the snow temperature profile in the NSL, snow surface temperature, surface snow grain size, and shortwave albedo; we compared these calculated values with in situ measurements. In the numerical simulation, the initial conditions of the snow were specified from the snow pit measurements conducted on 30 June 2012, 16:45 UTC. The SMAP model was subsequently driven by 5 min averaged meteorological data, including air pressure; air temperature; relative humidity; wind speed; and downward shortwave, near-infrared, and longwave radiant fluxes. The SMAP model was also driven by the daily temperature at the bottom of the thick ice layer in the NSL, the mass concentrations of snow impurities obtained every other day, and 5 min averaged accumulated precipitation based on 3 hourly ERA-Interim reanalysis data corrected by in situ bucket measurements.

Validation results revealed that the RMSE for the snow temperature profile and snow surface temperature were ~~comparable and~~ reasonable. Regarding surface snow grain size, simulation results were compared against GRS data obtained from spectral albedo measurements post-processed with a GSAF algorithm. Although the RMSE and ME that we obtained were comparable in magnitude to those reported from previous model validation studies performed at Sapporo, Japan, the small snow grain size associated with the surface hoar observed during 3–5 July could not be simulated by the SMAP model. In the SMAP model, surface hoar is created when H_L is positive and the wind speed is less than 3 m s^{-1}. However, the simulated H_L from the night of 2 July to the morning of 5 July was continuously negative. Despite these discrepancies, the simulated shortwave albedo was in reasonable agreement with observations throughout the IOP (RMSE $= 0.023$, and ME $= 0.008$). The cause of the agreement between the simulated shortwave albedo and observations, even during the 3–5 July period when the SMAP model could not reproduce surface hoar and associated small near-surface snow grain size, was a decrease of the near-infrared fraction of the downward shortwave radiant flux caused by the appearance of low-level clouds during the IOP. This change in the shortwave radiant flux increased the influence of visible albedo and in turn decreased the effect of near-infrared albedo on the shortwave albedo.

These physical processes are explicitly taken into account by the PBSAM, an important component of the SMAP model, highlighting that an advantage of PBSAM.

Because the method of calculating the H_L needed to be improved to obtain an accurate SEB in the validation of the snow grain size calculated with the SMAP model, we performed another numerical simulation with the SMAP model. In this simulation, 2-level data for air temperature, relative humidity, and wind speed were used to calculate H_L with the 2LM method, which calculated H_L from atmospheric profiles only and did not require the condition originally assumed by the SMAP model that the snow surface was saturated (1LM). In this case, the calculated H_L around 4 July turned positive, and the SMAP modelwas able to detect surface hoar deposition as well as simulate the associated small surface snow grain size. Because results from 1LM are affected by the choice of z_0, we performed numerical sensitivity tests, where values of z_0 were perturbed between the possible maximum and minimum values (10 and 0.01, respectively). As a result, we confirmed that characteristics of latent heat flux from 1LM is significantly different from that from 2LM. Based on these results, we could confirm that the 2LM method was an effective way to obtain an accurate H_L. Although it is presently quite common to run land surface models by forcing with 1-level meteorological data, the present results suggest that it is preferable to input 2-level atmospheric measurements (if available) into a physical snowpack model, because this method increases the likelihood of detecting surface hoar compared to the probability if 1-level atmospheric measurements are employed to drive the model.

Finally, we Using the SMAP model, we investigated the SEB at the SIGMA-A site during the IOP. Radiation-related components of the SEB were directly given from the AWS measurements, whereas other components , except for H_L, were calculated by the SMAP model as a function of measured snow surface temperature. The H_L was calculated with the 2LM method based on the results mentioned above. The calculated calculated SEB was clearly different between Period-1 (30 June to 9 July) and Period-2 (10 to 14 July): L_{net} increased dramatically by $+57.1\,W\,m^{-2}$ (H_S and H_L also increased by $+11.3$ and $+31.025.2\,W\,m^{-2}$, respectively) after 10 July, whereas S_{net} decreased significantly by $-42.3\,W\,m^{-2}$. Conse-

quently, Q_{net} clearly varied diurnally (negative during the night and positive during the day) until 9 July. However, the fact that it remained continuously positive after 10 July explains the continuous melt event observed at the SIGMA-A site. We discussed the reason for this remarkable transition of radiative properties, and we concluded that it was caused by the appearance of low-level clouds accompanied by a significant temperature increase. The result was surface heating during Period-2 via the process of cloud radiative forcing in the polar region.

In order to confirm the validity of SEB characteristics during IOP, additional error analyses were conducted. During this process, it was turned out that the sign of latent heat fluxes from the 1LM and 2LM methods differed especially when the surface hoar was observed (around 4 July). The former showed negative, while the latter turned positive and designated the surface hoar formation. Therefore, the 2LM method calculated latent heat flux seemed to be plausible; however, uncertainty involved in the 2LM method was so large that we could not confirm its significance.

Author contributions. M. Niwano developed the SMAP model code and performed the numerical calculations. T Aoki designed the SIGMA AWS system. T. Aoki, S. Matoba, S. Yamaguchi, T. Tanikawa, M. Niwano, K. Kuchiki, and H. Motoyama installed the SIGMA-A AWS on the GrIS and constructed data-acquisition system. S. Matoba and S. Yamaguchi performed snow pit measurements. T. Aoki and K. Kuchiki processed data of mass concentrations of snow impurities. M. Niwano, T. Aoki, and T. Tanikawa conducted spectral albedo measurements. K. Kuchiki retrieved GRS from the spectral albedo data. M. Niwano prepared the manuscript with contributions from all co-authors.

Acknowledgements. We sincerely thank Tetsuhide Yamasaki for logistical and field support of our expedition, and Sakiko Daorana for her help during our stay at Qaanaaq, Greenland. We thank Climatec Inc. (Japan) for manufacturing the AWS installed at the SIGMA-A site, and Masae Igosaki for supporting the laboratory measurements of snow impurities. We would like to thank two reviewers, John King and an anonymous referee, and the scientific editor of this paper, Michiel van den Broeke for their quite helpful comments and suggestions. This study was supported in part by (1) the Japan Society for the Promotion of Science (JSPS), Grant-in-Aid for Scientific Research (S), number 23221004, (2) the Global Change Observation Mission – Climate (GCOM-C)/the Second-generation GLobal Imager (SGLI) Mission, the Japan Aerospace Exploration Agency (JAXA), (3)

the Experimental Research Fund for Global Environment Conservation, the Ministry of the Environment of Japan, and (4) the Grant for Joint Research Program, the Institute of Low Temperature Science, Hokkaido University. The map showing the location of site SIGMA- A (Fig. 1) was created by NunaGIS (http://en.nunagis.gl/) operated by Asiaq, Greenland Survey.

References

Anderson, E. A.: A point energy and mass balance model of a snow cover, NOAA Tech. Rep. NWS19, Office of Hydrology, National Weather Service, Silver Spring, Maryland, US, 1976.

Anderson, P. S.: A method for rescaling humidity sensors at temperatures well below freezing, J. Atmos. Oceanic Technol., 11, 1388–1391, doi:10.1175/1520-0426(1994)011<1388:AMFRHS>2.0.CO;2, 1994.

Andreas, E. L.: A theory for the scalar roughness and the scalar transfer coefficients over snow and ice, Bound.-Lay- Meteorol., 38, 159–184, doi:10.1007/BF00121562, 1987.

Aoki, T. and Yamanouchi, T.: Cloud radiative forcing around Asuka Station, Antarctica, Proc. NIPR Symp. Polar Meteorol. Glaciol., 5, 76–89, 12–13 July 1990, Tokyo, 1992.

Aoki, T., Aoki, T., Fukabori, M., and Uchiyama, A.: Numerical simulation of the atmospheric effects on snow albedo with multiple scattering radiative transfer model for the atmosphere-snow system, J. Meteorol. Soc. Jpn., 77, 595–614, 1999.

Aoki, T., Aoki, T., Fukabori, M., Hachikubo, A., Tachibana, Y., and Nishio, F.: Effects of snow physical parameters on spectral albedo and bidirectional reflectance of snow surface, J. Geophys. Res., 105, 10219–10236, doi:10.1029/1999JD901122, 2000.

Aoki, T., Hachikubo, A., and Hori, M.: Effects of snow physical parameters on shortwave broadband albedos, J. Geophys. Res., 108, 4616, doi:10.1029/2003JD003506, 2003.

Aoki, T., Hori, M., Motoyoshi, H., Tanikawa, T., Hachikubo, A., Sugiura, K., Yasunari, T. J., Storvold, R., Eide, H. A., Stamnes, K., Li, W., Nieke, J., Nakajima, Y., and Takahashi, F.: ADEOS-II/GLI snow/ice products – Part II: Validation results using GLI and MODIS data, Remote Sens. Environ., 111, 274–290, doi:10.1016/j.rse.2007.02.035, 2007.

Aoki, T., Kuchiki, K., Niwano, M., Kodama, Y., Hosaka, M., and Tanaka, T.: Physically based snow albedo model for calculating broadband albedos and the solar heating profile in snowpack for general circulation models, J. Geophys. Res., 116, D11114, doi:10.1029/2010JD015507, 2011.

Aoki, T., Matoba, S., Uetake, J., Takeuchi, N., and Motoyama, H.: Field activities of the "Snow Impurity and Glacial Microbe effects on abrupt warming in the Arctic" (SIGMA) project in Greenland in 2011–2013, Bull. Glaciol. Res., 32, 3–20, doi:10.5331/bgr.32.3, 2014a.

Aoki, T., Matoba, S., Yamaguchi, S., Tanikawa, T., Niwano, M., Kuchiki, K., Adachi, K., Uetake, J., Motoyama, H., and Hori, M.: Light-absorbing snow impurity concentrations measured on Northwest Greenland ice sheet in 2011 and 2012, Bull. Glaciol. Res., 32, 21–31, doi:10.5331/bgr.32.21, 2014b.

Armstrong, R. L. and Brun, E. (Eds.): Snow and Climate: Physical Processes, Surface Energy Exchange and Modeling, Cambridge Univ. Press, Cambridge, UK, 2008.

Bennartz, R., Shupe, M. D., Turner, D. D., Walden, V. P., Steffen, K., Cox, C. J., Kulie, M. S., Miller, N. B., and Pettersen, C.: July 2012 Greenland melt extent enhanced by low-level liquid clouds, Nature, 496, 83–86, doi:10.1038/nature12002, 2013.

Bonne, J.-L., Steen-Larsen, H. C., Risi, C., Werner, M., Sodemann, H., Lacour, J.-L., Fettweis, X., Cesana, G., Delmotte, M., Cattani, O., Vallelonga, P., Kjær, H. A., Clerbaux, C., Sveinbjörnsdóttir, Á., E., and Masson-Delmotte, V.: The summer 2012 Greenland heat wave: In situ and remote sensing observations of water vapor isotopic composition during an atmospheric river event, J. Geophys. Res. Atmos., 120, doi:10.1002/2014JD022602, 2015.

Box, J. E. and Steffen, K.: Sublimation on the Greenland ice sheet from automated weather station observations, J. Geophys. Res., 106, 33965–33981, doi:10.1029/2001JD900219, 2001.

Box, J. E., Fettweis, X., Stroeve, J. C., Tedesco, M., Hall, D. K., and Steffen, K.: Greenland ice sheet albedo feedback: thermodynamics and atmospheric drivers, The Cryosphere, 6, 821–839, doi:10.5194/tc-6-821-2012, 2012.

Braithwaite, R. J.: Aerodynamic stability and turbulent sensible-heat flux over a melting ice surface, the Greenland ice sheet, J. Glaciol., 41, 562–571, 1995.

Brock, B. W., Willis, I. C., and Sharp, M. J.: Measurement and parameterization of aerodynamic roughness length variations at Haut Glacier d'Arolla, Switzerland, J. Glaciol., 52, 281–297, 2006.

Brun, E., Martin, E., Simon, V., Gendre, C., and Coleou, C.: An energy and mass model of snow cover suitable for operational avalanche forecasting, J. Glaciol., 35, 333–342, 1989.

Brun, E., David, P., Sudul, M., and Brunot, G.: A numerical model to simulate snow-cover stratigraphy for operational avalanche forecasting, J. Glaciol., 38, 13–22, 1992.

Brun, E., Six, D., Picard, G., Vionnet, V., Arnaud, L., Bazile, E., Boone, A., Bouchard, A., Genthon, C., Guidard, V., Le Moigne, P., Rabier, F., and Seity, Y.: Snow/atmosphere coupled simulation at Dome C, Antarctica, J. Glaciol., 52, 721–736, doi:10.3189/002214311797409794, 2011.

Carmagnola, C. M., Morin, S., Lafaysse, M., Domine, F., Lesaffre, B., Lejeune, Y., Picard, G., and Arnaud, L.: Implementation and evaluation of prognostic representations of the optical diameter of snow in the SURFEX/ISBA-Crocus detailed snowpack model, The Cryosphere, 8, 417–437, doi:10.5194/tc-8-417-2014, 2014.

Chen, L., Johannessen, O. M., Huijum, W., and Ohmura, A.: Accumulation over the Greenland Ice Sheet as represented in reanalysis data, Adv. Atmos. Sci., 28, 1–9, doi:10.1007/s00376-010-0150-9, 2011.

Cullen, N. J., and Steffen, K.: Unstable near-surface boundary conditions in summer on top of the Greenland Ice Sheet, Geophys. Res. Lett., 28, 4491–4493, doi:10.1029/2001GL013417, 2001.

Cullen, N. J., Mölg, T., Conway, J., and Steffen, K.: Assessing the role of sublimation in the dry snow zone of the Greenland ice sheet in a warming world, J. Geophys. Res. Atmos., 119, 6563–6577, doi:10.1002/2014JD021557, 2014.

Dadic, R., Schneebeli, M., Lehning, M., Hutterli, M. A., and Ohmura, A.: Impact of the microstructure of snow on its temperature: a model validation with measurements from Summit, Greenland, J. Geophys. Res., 113, D14303, doi:10.1029/2007JD009562, 2008.

Dee, D. P., Uppala, S. M., Simmons, A. J., Berrisford, P., Poli, P., Kobayashi, S., Andrae, U., Balmaseda, M. A., Balsamo, G., Bauer, P., Bechtold, P., Beljaars, A. C. M., van de Berg, L., Bidlot, J., Bormann, N., Delsol, C., Dragani, R., Fuentes, M., Geer, A. J., Haimberger, L., Healy, S. B., Hersbach, H., Hólm, E. V., Isaksen, L., Kållberg, P., Köhler, M., Matricardi, M., McNally, A. P., Monge-Sanz, B. M., Morcrette, J.-J., Park, B.-K., Peubey, C., de Rosnay, P., Tavolato, C., Thépaut, J.-N., and Vitart, F.: The ERA-Interim reanalysis: configuration and performance of the data assimilation system, Q. J. Roy. Meteor. Soc., 137, 553–597, doi:10.1002/qj.828, 2011.

Fettweis, X., Tedesco, M., van den Broeke, M., and Ettema, J.: Melting trends over the Greenland ice sheet (1958–2009) from spaceborne microwave data and regional climate models, The Cryosphere, 5, 359–375, doi:10.5194/tc-5-359-2011, 2011.

Fettweis, X., Hanna, E., Lang, C., Belleflamme, A., Erpicum, M., and Gallée, H.: *Brief communication* "Important role of the mid-tropospheric atmospheric circulation in the recent surface melt increase over the Greenland ice sheet", The Cryosphere, 7, 241–248, doi:10.5194/tc-7-241-2013, 2013.

Fierz, C., Armstrong, R. L., Durand, Y., Etchevers, P., Greene, E., McClung, D. M., Nishimura, K., Satyawali, P. K., and Sokratov, S. A.: The International Classification for Seasonal Snow on the Ground, IHP-VII Technical Documents in Hydrology N_83, IACS Contribution N_1, UNESCO-IHP, Paris, viii, 80 pp., 2009.

Föhn, P. M. B.: Simulation of surface-hoar layers for snow-cover models, Ann. Glaciol., 32, 19–26, doi:10.3189/172756401781819490, 2001.

Giesen R. H., Andreassen, L. M., Oerlemans, J., and van den Broeke, M. R.: Surface energy balance in the ablation zone of Langfjordjøkelen, an arctic, maritime glacier in northern Norway, J. Glaciol., 60, 57–70, doi:10.3189/2014JoG13J063, 2014.

Goudriaan, J.: Crop Micrometeorology: A Simulation Study, Pudoc, Wageningen, Netherlands, 1977.

Greuell, W. and Konzelmann, T.: Numerical modelling of the energy balance and the englacial temperature of the Greenland Ice Sheet. Calculations for the ETH-Camp location (West Greenland, 1155 m a.s.l.), Global Planet. Change, 9, 91–114, doi:10.1016/0921-8181(94)90010-8, 1994.

Hall, D. K., Comiso, J. C., DiGirolamo, N. E., Shuman, C. A., Box, J. E., and Koenig, L. S.: Variability in the surface temperature and melt extent of the Greenland ice sheet from MODIS, Geophys. Res. Lett., 40, 2114–2120, doi:10.1002/grl.50240, 2013.

Hanna, E., Fettweis, X., Mernild, S. H., Cappelen, J., Ribergaard, M. H., Shuman, C. A., Steffen, K., Wood, L., and Mote, T. L.: Atmospheric and oceanic climate forcing of the exceptional Greenland ice sheet surface melt in summer 2012, Int. J. Climatol., 34, 1022–1037, doi:10.1002/joc.3743, 2014.

Hirashima, H., Yamaguchi, S., Sato, A., and Lehning, M.: Numerical modeling of liquid water movement through layered snow based on new measurements of the water retention curve, Cold Reg. Sci. Technol., 64, 94–103, doi:10.1016/j.coldregions.2010.09.003, 2010.

Holtslag, A. A. M., and De Bruin, H. A. R.: Applied modeling of the nighttime surface energy balance over land, J. Appl. Meteorol., 27, 689–704, doi:10.1175/1520-0450(1988)027<0689:AMOTNS>2.0.CO;2, 1988.

Ishimoto, H., Masuda, K., Mano, Y., Orikasa, N., and Uchiyama, A.: Irregularly shaped ice aggregates in optical modeling of convectively generated ice clouds, J. Quant. Spectrosc. Ra., 113, 632–643, doi:10.1016/j.jqsrt.2012.01.017, 2012.

Khan, S. A., Wahr, J., Bevis, M., Velicogna, I., and Kendrick, E.: Spread of ice mass loss into northwest Greenland observed by GRACE and GPS, Geophys. Res. Lett., 37, L06501, doi:10.1029/2010GL042460, 2010.

King, J. C., Gadian, A., Kirchgaessner, A., Kuipers Munneke, P., Lachlan-Cope, T. A., Orr, A., Reijmer, C., van den Broeke, M. R., van Wessem, J. M., and Weeks, M.: Validation of the summertime surface energy budget of Larsen C Ice Shelf (Antarctica) as represented in three high-resolution atmospheric models. J. Geophys. Res. Atmos., 120, 1335–1347, doi:10.1002/2014JD022604, 2015.

Kuchiki, K., Aoki, T., Tanikawa, T., and Kodama, Y.: Retrieval of snow physical parameters using a ground-based spectral radiometer, Appl. Optics, 48, 5567–5582, doi:10.1364/AO.48.005567, 2009.

Kuipers Munneke, P., van den Broeke, M. R., Reijmer, C. H., Helsen, M. M., Boot, W., Schneebeli, M., and Steffen, K.: The role of radiation penetration in the energy budget of the snowpack at Summit, Greenland, The Cryosphere, 3, 155–165, doi:10.5194/tc-3-155-2009, 2009.

Kuipers Munneke, P., van den Broeke, M. R., King, J. C., Gray, T., and Reijmer, C. H.: Near-surface climate and surface energy budget of Larsen C ice shelf, Antarctic Peninsula, The Cryosphere, 6, 353–363, doi:10.5194/tc-6-353-2012, 2012.

Lehning, M., Bartelt, P., Brown, B., Fierz, C., and Satyawali, P.: A physical SNOWPACK model for the Swiss avalanche warning. Part II: Snow microstructure, Cold Reg. Sci. Technol., 35, 147–167, doi:10.1016/S0165-232X(02)00073-3, 2002.

Liljequist, G. H.: Energy Exchanges of an Antarctic Snow-Field: Short-Wave Radiation, Norwegian-British-Swedish Antarctic Expedition (Maudheim, 71°03′ S, 10°56′ W), 1949–52, Scientific Results, Vol. 2, Part 1A, Norsk Polarinstitutt, Oslo, 107 pp., 1956.

Neff, W., Compo, G. P., Ralph, F. M., and Shupe, M. D.: Continental heat anomalies and the extreme melting of the Greenland ice surface in 2012 and 1889, J. Geophys. Res. Atmos., 119, 6520–6536, doi:10.1002/2014JD021470, 2014.

Nghiem, S. V., Hall, D. K., Mote, T. L., Tedesco, M., Albert, M. R., Keegan, K., Shuman, C. A., DiGirolamo, N. E., and Neumann, G.: The extreme melt across the Greenland ice sheet in 2012, Geophys. Res. Lett., 39, L20502, doi:10.1029/2012GL053611, 2012.

Niwano, M., Aoki, T., Kuchiki, K., Hosaka, M., and Kodama, Y.: Snow Metamorphism and Albedo Process (SMAP) model for climate studies: model validation using meteorological and snow impurity data measured at Sapporo, Japan, J. Geophys. Res., 117, F03008, doi:10.1029/2011JF002239, 2012.

Niwano, M., Aoki, T., Kuchiki, K., Hosaka, M., Kodama, Y., Yamaguchi, S., Motoyoshi, H., and Iwata, Y.: Evaluation of updated physical snowpack model SMAP, Bull. Glaciol. Res., 32, 65–78, doi:10.5331/bgr.32.65, 2014.

Ohmura, A., and Reeh, N.: New precipitation and accumulation maps for Greenland, J. Glaciol., 37, 140–148, 1991.

Ohmura, A., Konzelmann, T., Rotach, M., Forrer, J., Wild, M., Abe-Ouchi, A., and Toritani, H.: Energy balance for the Greenland ice sheet by observation and model computation, in: Snow and Ice

Covers; Interaction With the Atmosphere and Ecosystems, Jones, H. G., Davies, T. D., Ohmura, A., Morris, E. M. (Eds.), IAHS, Gentbrugge, Belgium, 85–94, 1994.

Paulson, C. A.: The mathematical representation of wind speed and temperature profiles in the unstable atomospheric surface layer, J. Appl. Meteorol., 9, 857–861, doi:10.1175/1520-0450(1970)009<0857:TMROWS>2.0.CO;2, 1970.

Pinzer, B. R. and Schneebeli, M.: Snow metamorphism under alternating temperature gradients: morphology and recrystallization in surface snow, Geophys. Res. Lett., 36, L23503, doi:10.1029/2009GL039618, 2009.

Richards, L. A.: Capillary conduction of liquids through porous mediums, J. Appl. Phys., 1, 318–333, doi:10.1063/1.1745010, 1931.

Shimizu, H.: Air Permeability of Deposited Snow, Contributions from the Institute of Low Temperature Science, A22, 1–32, Institute of Low Temperature Science, Hokkaido University, Sapporo, Japan, 1970.

Smeets, C. J. P. P. and van den Broeke, M. R.: Temporal and spatial variations of the aerodynamic roughness length in the ablation zone of the Greenland ice sheet, Bound.-Lay. Meteorol., 128, 315–338, doi:10.1007/s10546-008-9291-0, 2008.

Steffen, K., and Box, J.: Surface climatology of the Greenland Ice Sheet: Greenland Climate Network 1995–1999, J. Geophys. Res., 106(D24), 33951–33964, doi:10.1029/2001JD900161, 2001.

Tedesco, M., Fettweis, X., Mote, T., Wahr, J., Alexander, P., Box, J. E., and Wouters, B.: Evidence and analysis of 2012 Greenland records from spaceborne observations, a regional climate model and reanalysis data, The Cryosphere, 7, 615–630, doi:10.5194/tc-7-615-2013, 2013.

van As, D.: Warming, glacier melt and surface energy budget from weather station observations in the Melville Bay region of northwest Greenland, J. Glaciol., 57, 208–220, doi:10.3189/002214311796405898, 2011.

van den Broeke, M., Reijmer, C., and van de Wal, R.: Surface radiation balance in Antarctica as measured with automatic weather stations, J. Geophys. Res., 109, D09103, doi:10.1029/2003JD004394, 2004.

van den Broeke, M., Reijmer, C., van As, D., van de Wal, R., and Oerlemans, J.: Seasonal cycles of Antarctic surface energy balance from automatic weather stations, Ann. Glaciol., 41, 131–139, 2005.

van den Broeke, M., Reijmer, C., van As, D., and Boot, W.: Daily cycle of the surface energy balance in Antarctica and the influence of clouds, Int. J. Climatol., 26, 1587–1605, doi:10.1002/joc.1323, 2006.

van den Broeke, Smeets, P., and Ettema, J.: Surface layer climate and turbulent exchange in the ablation zone of the west Greenland ice sheet, Int. J. Climatol., 29, 2309–2323, doi:10.1002/joc.1815, 2009.

van den Broeke, M. R., Smeets, C. J. P. P., and van de Wal, R. S. W.: The seasonal cycle and interannual variability of surface energy balance and melt in the ablation zone of the west Greenland ice sheet, The Cryosphere, 5, 377–390, doi:10.5194/tc-5-377-2011, 2011.

van Genuchten, M. T.: A closed-form equation for predicting the hydraulic conductivity of unsaturated soil, Soil Sci. Soc. Am. J., 44, 892–898, 1980.

Vionnet, V., Brun, E., Morin, S., Boone, A., Faroux, S., Le Moigne, P., Martin, E., and Willemet, J.-M.: The detailed snowpack scheme Crocus and its implementation in SURFEX v7.2, Geosci. Model Dev., 5, 773–791, doi:10.5194/gmd-5-773-2012, 2012.

Wiscombe, W. J. and Warren, S. G.: A model for the spectral albedo of snow. I: Pure snow, J. Atmos. Sci., 37, 2712–2733, doi:10.1175/1520-0469(1980)037<2712:AMFTSA>2.0.CO;2, 1980.

Yamaguchi, S., Katsushima, T., Sato, A., and Kumakura, T.: Water retention curve of snow with different grain sizes, Cold Reg. Sci. Technol., 64, 87–93, doi:10.1016/j.coldregions.2010.05.008, 2010.

Yamaguchi, S., Watanabe, K., Katsushima, T., Sato, A., and Kumakura, T.: Dependence of the water retention curve of snow on snow characteristics, Ann. Glaciol., 53, 6–12, doi:10.3189/2012AoG61A001, 2012.

Yamaguchi, S., Matoba, S., Yamazaki, T., Tsushima, A., Niwano, M., Tanikawa, T., and Aoki, T.: Glaciological observations in 2012 and 2013 at SIGMA-A site, Northwest Greenland, Bull. Glaciol. Res., 32, 95–105, doi:10.5331/bgr.32.95, 2014.

Yamanouchi, T.: Variations of incident solar flux and snow albedo on the solar zenith angle and cloud cover, at Mizuho station, Antarctica, J. Meteorol. Soc. Jpn., 61, 879–893, 1983.

Yamazaki, T.: A one-dimensional land surface model adaptable to intensely cold regions and its applications in eastern Siberia, J. Meteorol. Soc. Jpn., 79(6), 1107–1118, doi:10.2151/jmsj.79.1107, 2001.

Yukimoto, S., Yoshimura, H., Hosaka, M., Sakami, T., Tsujino, H., Hirabara, M., Tanaka, T. Y., Deushi, M., Obata, A., Nakano, H., Adachi, Y., Shindo, E., Yabu, S., Ose, T., and Kitoh, A.: Meteorological Research Institute Earth System Model Version 1 (MRI-ESM1) – Model Description, Tech. Rep. of MRI, 64, 83 pp., available at: http://www.mri-jma.go.jp/Publish/Technical/index_en.html, 2011.

Table 1. Comparison of SMAP simulation results with in situ measurements. RMSE and ME are the root mean square error and mean error (the average of the difference between simulated values and observed values), respectively. Figures in parentheses indicate scores when the observed surface temperature was negative (i.e., dry snow conditions).

Parameters	RMSE	ME
Snow temperature profile (°C)	~~0.59 (0.80~~0.60 (0.81)	−0.16 (−~~0.23~~0.24)
Snow surface temperature (°C)	~~0.53 (0.85~~0.58 (0.94)	~~0.21 (0.55~~0.25 (0.68)
Surface snow grain size (mm)	0.21	~~0.16~~ 0.17
Shortwave albedo	~~0.023~~0.022	0.008

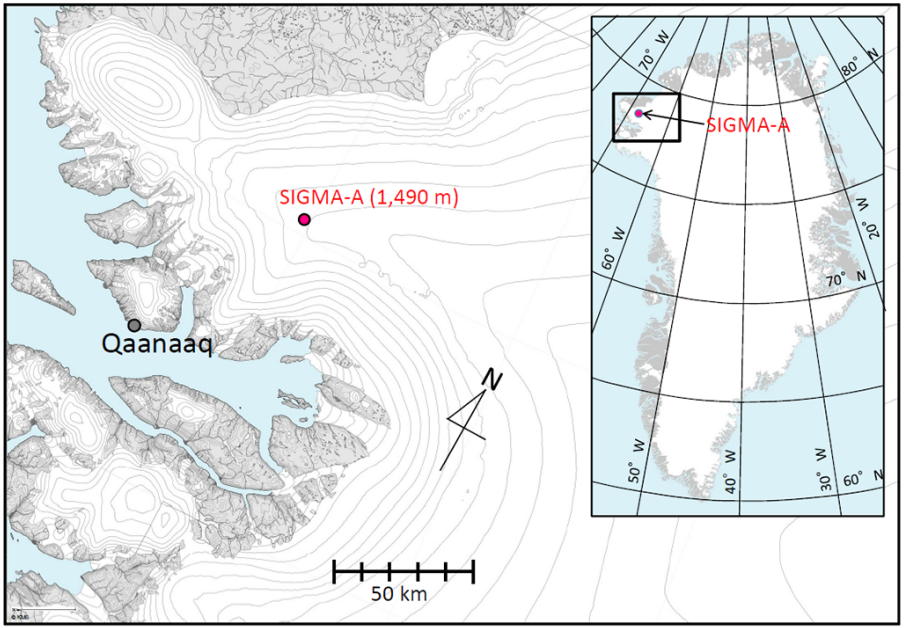

Figure 1. The location of site SIGMA-A together with ice sheet surface elevation contours (m a.s.l.). Height interval is 100 m.

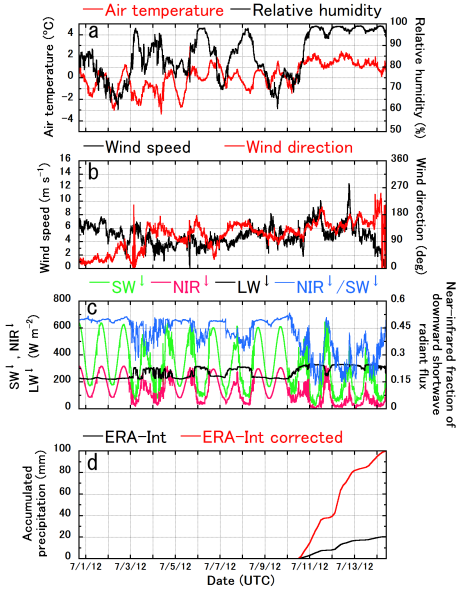

Figure 2. Meteorological conditions measured at SIGMA-A during the IOP (30 June to 14 July 2012): **(a)** air temperature and relative humidity with respect to water observed at a nominal height of 3.0 m above the snow surface~~on 29 June 2012~~; **(b)** wind speed and direction observed at 3.0 m above the snow surface on 29 June 2012 (Wind direction is denoted in degrees that indicate the direction from which the wind is blowing. The degrees increase from 0 to 360 as the direction is rotated clockwise from north.); **(c)** downward shortwave ($SW^{\downarrow}$), near-infrared ($NIR^{\downarrow}$), longwave ($LW^{\downarrow}$) radiant fluxes, and the near-infrared fraction of the $SW^{\downarrow}$; and **(d)** accumulated precipitation obtained from 3 hourly ERA-Interim reanalysis data (ERA-Int), where the black line denotes the original amount of precipitation and the red line reflects the correction based on in situ measurements of accumulated precipitation measured during the period from 20:00 UTC on 12 July 2012 to 11:00 UTC on 14 July 2012.

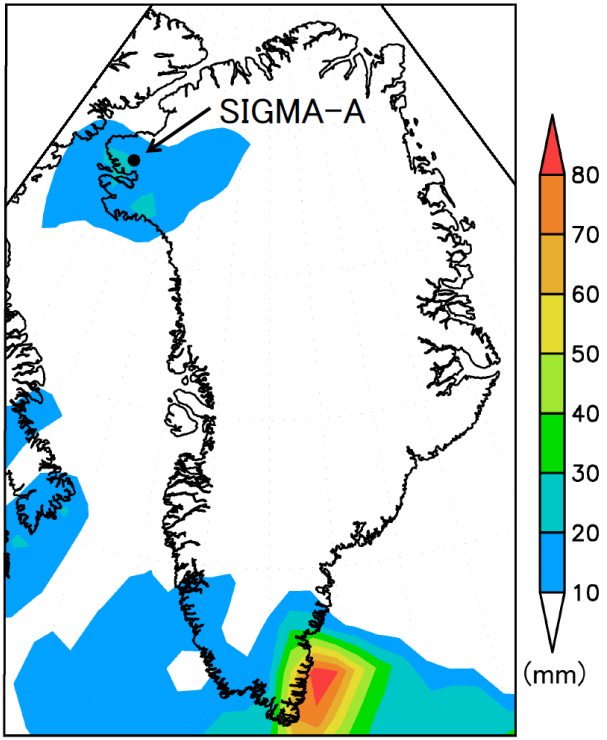

Figure 3. Accumulated precipitation from 00:00 UTC on 10 July 2012 to 12:00 UTC on 14 July 2012 obtained from the 3 hourly ERA-Interim reanalysis data. Black colored circle indicates the location of site SIGMA-A.

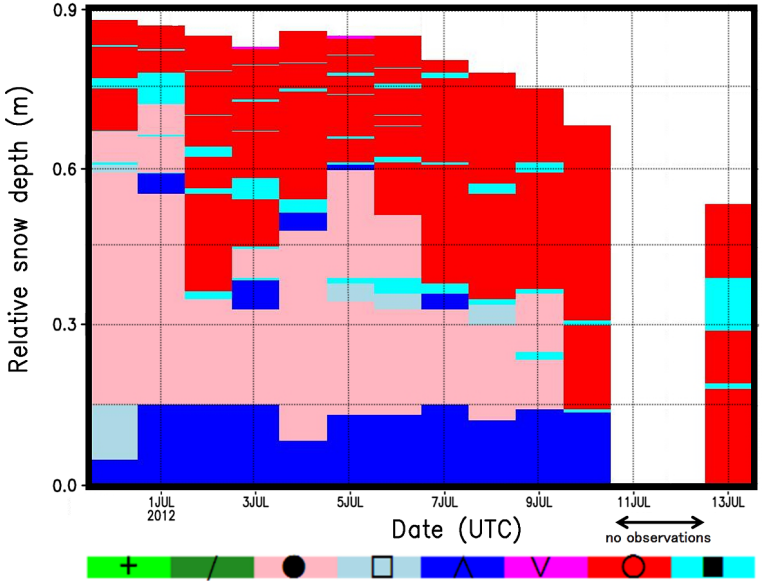

Figure 4. Temporal evolution of observed main snow grain shape profile within the NSL, which was defined by a thick bottom ice layer, at SIGMA-A during the IOP. Vertical axis (relative snow depth) denotes the height above the bottom thick ice layer. Characters and colors indicating snow grain shape follow the definition by Fierz et al. (2009). In sequence from the left they denote precipitation particles, decomposing and fragmented precipitation particles, rounded grains, faceted crystals, depth hoar, surface hoar, melt forms, and ice layer.

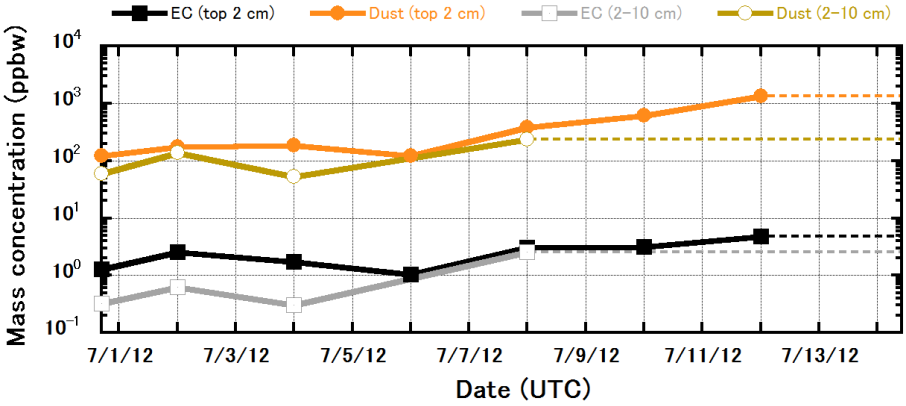

Figure 5. Measured mass concentrations of elemental carbon (EC) and dust in the top 2 cm of snow layers and the subsurface (2–10 cm) layers at the SIGMA-A site during the IOP. Dashed lines indicate periods when there were no measurements.

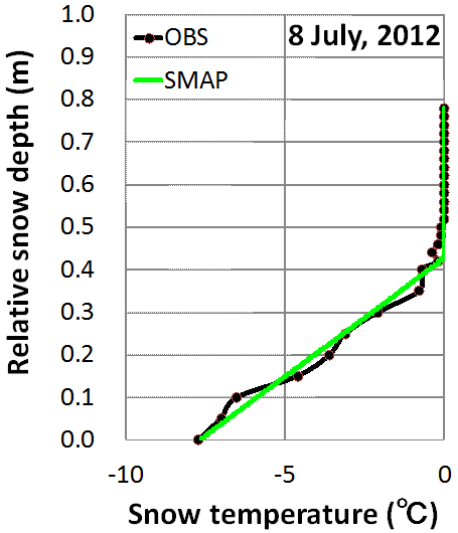

Figure 6. Comparison of snow temperature profiles in the NSL at the SIGMA-A site between snow pit observations (OBS) and profiles simulated with the SMAP model at 11:30 UTC on 8 July 2012. Relative snow depth denotes the height of the NSL above the thick bottom layer of ice. The snow depths simulated by the SMAP model were adjusted to the measurements.

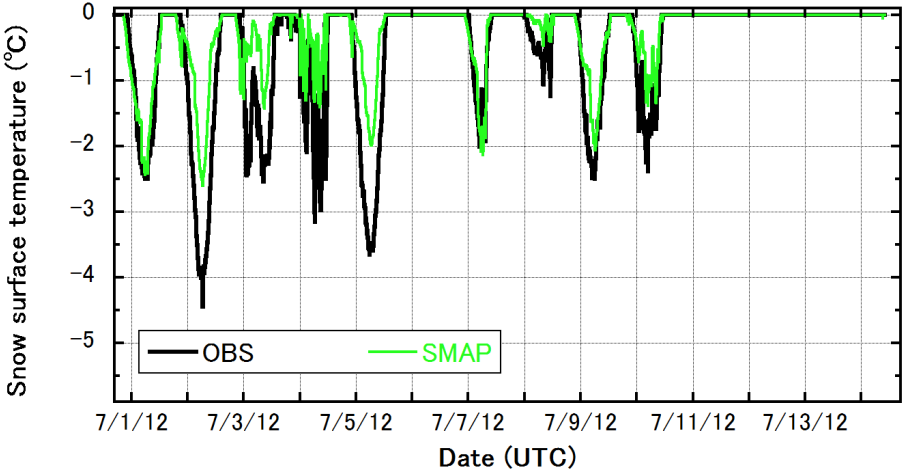

Figure 7. Snow surface temperature at the SIGMA-A site during the IOP observed with the AWS and simulated by the SMAP model. Observed snow surface temperature was calculated from observed downward and upward longwave radiant fluxes (Sect. 4).

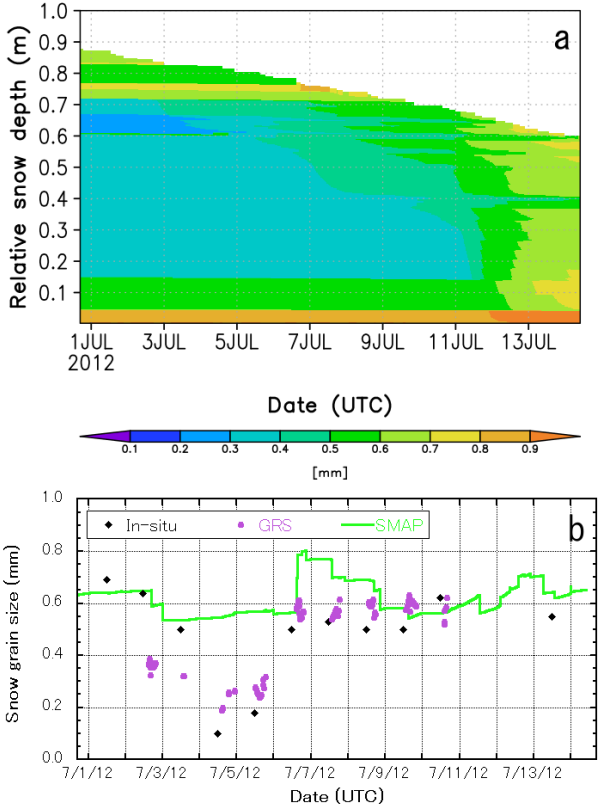

Figure 8. Temporal evolution of **(a)** simulated snow grain size profile in the NSL, and **(b)** surface snow grain size from in situ snow pit observations (black diamond patterns), ground-based remote sensing (GRS) using spectral albedo data measured with a spectrometer (purple dots), and simulated by the SMAP model (solid green curve) at the SIGMA-A site during the IOP. Vertical axis in the upper panel (relative snow depth) denotes the height above the thick bottom ice layer in the NSL.

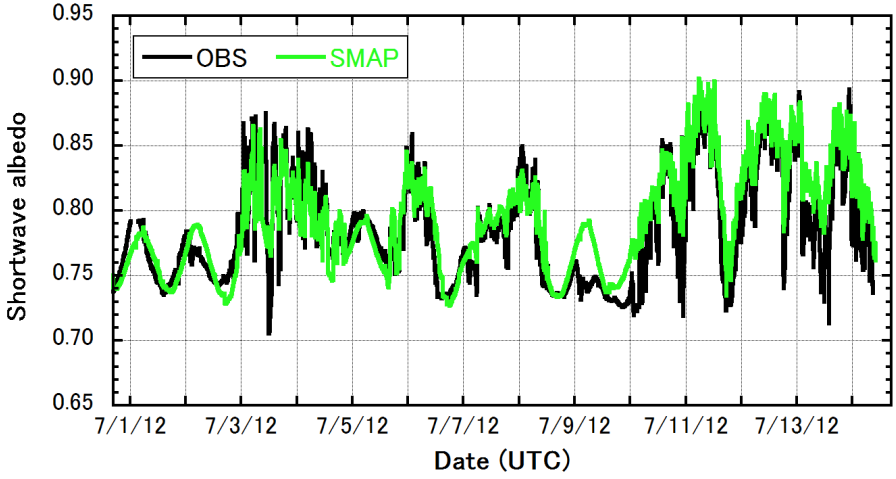

Figure 9. Shortwave albedos at the SIGMA-A site during the IOP observed with AWS and simulated by the SMAP model.

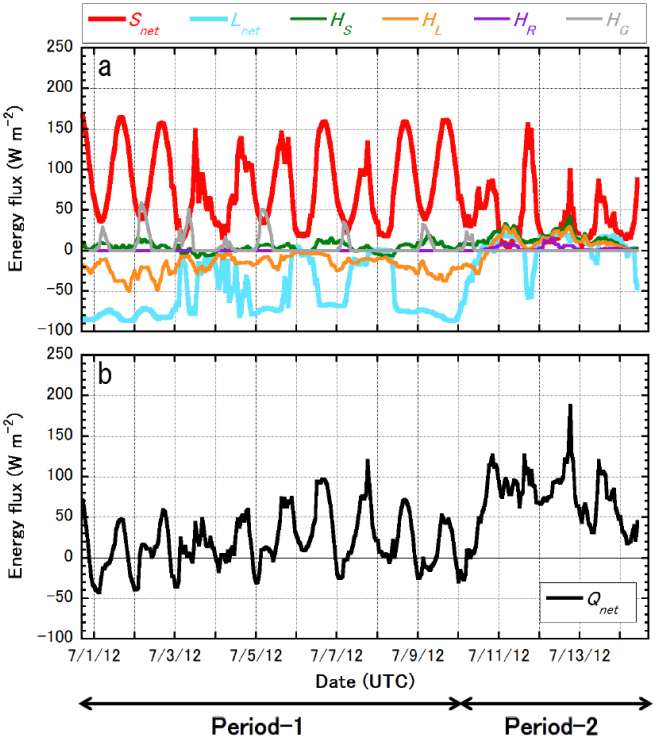

Figure 10. ~~One-hour averaged surface energy balance at the SIGMA-A site during the IOP. The upper panel **(a)** shows net shortwave radiant flux (S_{net}), net longwave radiant flux (L_{net}), sensible heat flux (H_{S}), latent heat flux (H_{L}), heat supply by rainfall (H_{R}), and subsurface conductive heat flux (H_{G}). These fluxes are defined to be positive when they are directed into the snow surface. The lower panel **(b)** denotes net energy flux (Q_{net}). The snow surface is heated when Q_{net} is positive, whereas it is cooled if Q_{net} is negative.~~ **(a)** Temporal evolution of 1 h averaged latent heat fluxes calculated from atmospheric measurements at 6 and 3 m above the surface (OBS_2LM) and measurements at 3 m above the surface (OBS_1LM), as well as the SMAP simulation forced by 1-level (3 m above the surface) atmospheric measurements (SMAP_1LM). **(b)** Comparison of 1 h averaged latent heat flux from OBS_1LM with those from two sensitivity tests, where z_0 are changed to be 0.01 and 10 mm from default OBS_1LM setting. **(c)** Comparison of surface snow grain size at the SIGMA-A site during the IOP with surface snow grain size from ground-based remote sensing (GRS) using spectral albedo data measured with a spectrometer and those from the SMAP simulations driven by 2-level (6 and 3 m above the surface) atmospheric measurements (SMAP_2LM) or 1-level (3 m above the surface) atmospheric measurements (SMAP_1LM).

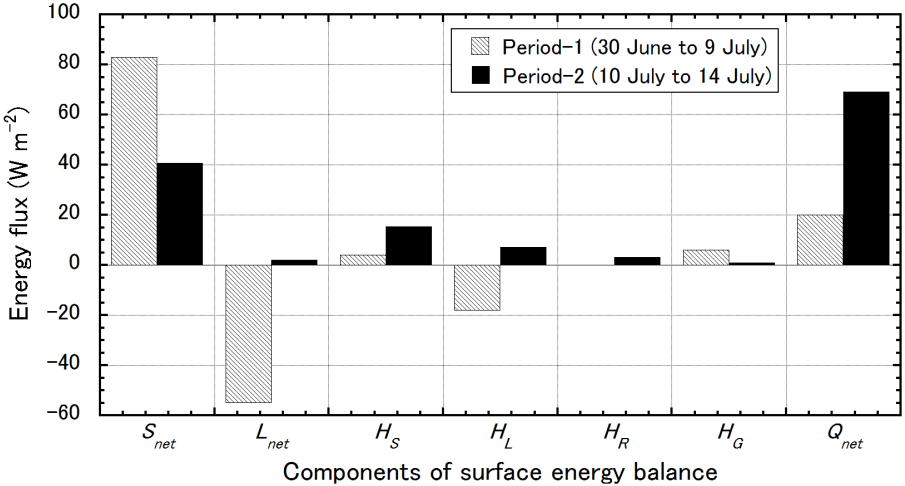

Figure 11. ~~Comparison of average surface energy balance components (S_{net}: net shortwave radiant flux, L_{net}: net longwave radiant flux, H_S: sensible heat flux, H_L: latent heat flux, H_R: heat supply by rainfall, H_G: subsurface conductive heat flux, and Q_{net}: net energy flux) between Period-1 and Period-2 at the SIGMA-A site.~~ One-hour averaged surface energy balance at the SIGMA-A site during the IOP. The upper panel **(a)** shows net shortwave radiant flux (S_{net}), net longwave radiant flux (L_{net}), sensible heat flux (H_S), latent heat flux (H_L), heat supply by rainfall (H_R), and subsurface conductive heat flux (H_G). These fluxes are defined to be positive when they are directed into the snow surface. The lower panel **(b)** denotes net energy flux (Q_{net}). The snow surface is heated when Q_{net} is positive, whereas it is cooled if Q_{net} is negative.

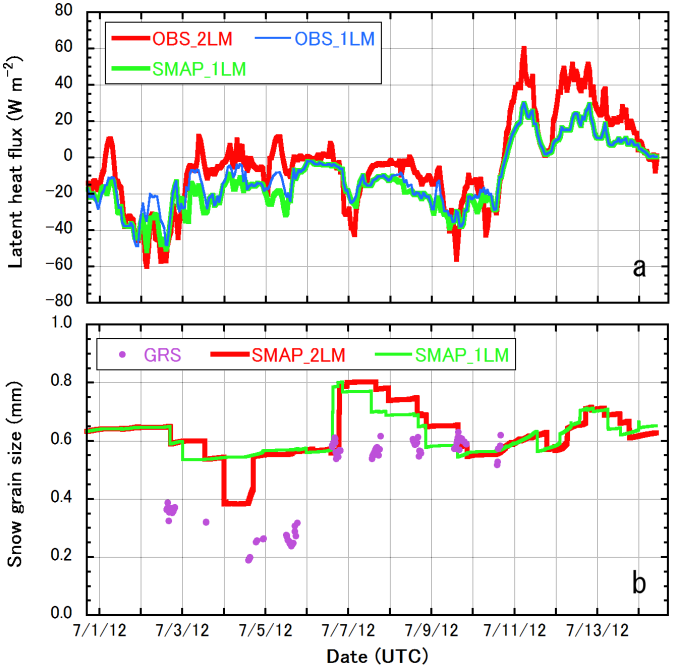
OBS_2LM
OBS_1LM
SMAP_1LM
Latent heat flux (W m^{-2})
80
60
40
20
0
−20
−40
−60
−80
a
GRS
SMAP_2LM
SMAP_1LM
Snow grain size (mm)
1.0
0.8
0.6
0.4
0.2
0.0
b
7/1/12
7/3/12
7/5/12
7/7/12
7/9/12
7/11/12
7/13/12
Date (UTC)

Figure 12. ~~**(a)** Temporal evolution of 1 h averaged latent heat fluxes calculated from atmospheric measurements at 6 and 3 m above the surface (OBS_2LM) and measurements at 3 m above the surface (OBS_1LM), as well as the SMAP simulation forced by 1-level (3 m above the surface) atmospheric measurements (SMAP_1LM). **(b)** Comparison of surface snow grain size at the SIGMA-A site during the IOP with surface snow grain size from ground-based remote sensing (GRS) using spectral albedo data measured with a spectrometer and those from the SMAP simulations driven by 2-level (6 and 3 m above the surface) atmospheric measurements (SMAP_2LM) or 1-level (3 m above the surface) atmospheric measurements (SMAP_1LM).~~ Comparison of average surface energy balance components (S_{net}: net shortwave radiant flux, L_{net}: net longwave radiant flux, H_{S}: sensible heat flux, H_{L}: latent heat flux, H_{R}: heat supply by rainfall, H_{G}: subsurface conductive heat flux, and Q_{net}: net energy flux) between Period-1 and Period-2 at the SIGMA-A site.